Wire gaseous coordinate detectors and their applications in biomedical research

V. D. Peshekhonov

Joint Institute for Nuclear Research, Dubna

Fiz. Elem. Chastits At. Yadra 17, 1030–1078 (September–October 1986)

Wire gaseous coordinate detectors continue to be a basic tool in experimental high-energy physics and are being intensively introduced into related areas of science and technology, particularly biomedical research. The constant evolution of these detectors allows broad application of their new modificatons: multistep chambers, low-pressure detectors, time-projection chambers, and so on, so that detector systems are enriched with new possibilities. In this review we give the operating principles and fundamental parameters of these detectors and discuss some examples of how they are used in experimental physics. We also explore some of the features of the use of these detectors for research in molecular biology and medical diagnostics for examples of existing and projected setups.

INTRODUCTION

The appearance of new charged-particle coordinate detectors—filmless wire spark counters, and then multiwire proportional chambers (MWPC) and drift chambers (DC)—in the 1960s in physics experiments at accelerators was largely due to the rapid development of microelectronics, electronic computational techniques, and standard electronic modular systems. These detectors then became one of the basic tools of high-energy physics, owing to their good space-time resolution characteristics, the possibility of using them for particle identification by means of ionization measurements, and the relative ease of preparing them according to the requirements of a particular experiment. This class of detectors now includes various modifications of time-projection chambers, two- and one-coordinate wire detectors operating in the self-quenched streamer (SQS) mode, and multistep shower chambers. A promising direction in the development of radiation detection techniques is based on the combination of wire gaseous detectors with detectors of other types.

The arsenal of detecting setups used in experimental nuclear physics is constantly being enlarged by new types of detectors with better spatial or time resolution. The new BGO and BaF_2 scintillators have been developed, and microchannel plates, silicon planar detectors, and devices with charge coupling have been put into operation. Nevertheless, the importance of gaseous coordinate detectors has not been diminished. For example, in the DELFI setup designed for experiments in the colliding electron–positron beams of LEP (at CERN) information will be recorded via $\sim 1.2\times 10^5$ channels from various detectors of this type, which amounts to about 75% of the proposed total number of detection channels.[1]

The existence of relatively inexpensive electronic computational installations equipped with a sufficient amount of fast memory together with the development of cathode readout techniques with MWPC and DC, which has made it possible to obtain two-coordinate information in the detection of neutrons and γ rays, has opened up the possibility of using these detectors as the so-called electronic analog of x-ray film. Studies in this direction were begun in the mid-1970s and are being carried out at many large physics centers such as CERN, JINR, the Institute of Nuclear Physics at Novosibirsk, and others. They are concentrating mainly on the application of MWPC to x-ray structural studies and medical diagnostics. The replacement of the traditional detectors by electronic ones allows the following:

1. The current techniques of obtaining and storing data can be used relatively simply, mathematical analyses of any complexity can be carried out, and the results can be presented in the form familiar to investigators.

2. The sensitivity can be increased by the improved radiation-detection efficiency and the significantly smaller background, thereby lowering the amount of radiation to which the objects under study are exposed and decreasing the investigation time by more than a factor of one hundred.

Aspects of the technique of gaseous coordinate detectors and features of their application in nuclear physics and applied research have been discussed in Refs. 2–7. The present article is devoted to a review of the principal features of these detectors and to some aspects of their application in biomedical research.

1. GASEOUS COORDINATE DETECTORS FOR DIGITAL RADIOGRAPHY IN BIOMEDICAL RESEARCH

The experience gained in the use of gaseous coordinate detectors in high-energy physics has shown that these detectors have the following main features:

1. The detectors can be controlled, so that the number of background events can be minimized.

2. They are useful for carrying out a preliminary selection of events.

3. They possess high time resolution (short memory time), so that particles separated from each other by very short time intervals can be distinguished.

4. Their dead time is short, that is, since they have a short response time, rapid data accumulation is ensured.

5. They possess fairly high spatial resolution, that is, the true coordinates of the points at which particles intersect the detector plane are determined accurately, and also they are

 0090-4759/86/050456-23$04.40

capable of detecting nearby events which occur simultaneously.

These detectors can be classified as detectors of the discrete or analog type, depending on their method of information readout.[8,9] In the first case the coordinate information is determined from the number of the discrete element of the detector whose electronics have recorded a pulse from the passage of a particle. In the second case the coordinates are determined via one of the following procedures: (a) by analysis of the detected charges according to the signals from several electronic circuits connected in parallel to the detector; (b) by measurement of the delay of the appearance of the signal relative to the time that the particle has passed through, which in turn is determined from the time for the produced charge to drift to the detection electronics; (c) by measurement of the signal delay time by means of the introduction of delay lines (DL) between discrete elements of the detector.

In high-energy physics only part of the radiation passing through the detector is of interest. When these detectors are used in applied research, it is assumed that all the detected radiation is of interest.

The structure of various objects is traditionally studied by obtaining the image of the object on photographic film or by detecting radiation passing through the object or emitted by it. The electronic coordinate detectors, for example, MPWC, used for such purposes together with their electronic instrumentation are referred to as electronic analogs of x-ray film, while the technique itself is called digital radiography. Here the detector might be of the form of a matrix of square cells, usually with from 64×64 to 256×256 cells. The amount of information sent to memory from these cells is from 4 to 64 K words, respectively. The linear dimensions of the cells (l_x and l_y), which determine the spatial resolution of the system, are usually 0.5 mm or larger. The relation $l_x l_y = S/N$ holds, where S is the sensitive area of the detector and N is the size of the memory, whose word capacity (up to 20 bytes) determines the dynamical range of the system. The characteristics of the system are determined by the detector, the method of information readout, and the electronic detection apparatus, which allows preliminary data selection and digital coding of the coordinate information. A computer with memory capabilities (buffer memory, magnetic tapes, floppy disks) is used for the storage, statistical analysis, digital processing, and final presentation of the information. Cathode-ray tube displays with the number of resolving elements no less than the number of detector cells and with a wide range of black/white or color gradiations are used to present the data.

A high intensity of the radiation flux and large information density require a fast detector and nullify the requirement that the detection be 100% efficient. Usually the efficiency is tens of percent and a high degree of uniformity in the area of the detector is ensured. A large angular spread of the radiation flux makes it necessary to use relatively thin detectors. The simplest and most widely used method of coordinate information readout in the case of MWPC detectors is based on the use of DL, which gives high resolution (a fraction of a millimeter) and faster operation (hundreds of kilohertz). We note that information readout from two ends of the DL leads to an increase in the spatial resolution by a factor of two without changing the time resolution. As a rule, the anode wires are connected and the signals from them are used to trigger the apparatus and to carry out event selection on the basis of the amplitude. The coordinate information is read out via two detection channels per coordinate.

When detectors are used in applied research, it is assumed that nonspecialists will be operating them. Consequently, the detector parameters should have a high degree of stability, the number of detection channels should be small, and the detector should be as simple as possible to use. Gaseous coordinate detectors come closest to satisfying these requirements.

2. RADIATION DETECTION. THE CHARGE COLLECTION MECHANISM

Charged radiation

When charged particles pass through matter, their electromagnetic interaction with the electrons and nuclei leads to excitation and ionization of the atoms which are important even in thin layers of matter. This ionization bremsstrahlung, which is important for slow particles, is accompanied by a decrease of the particle kinetic energy. The ionization losses per unit path length are given by the well-known Bethe–Bloch formula. The ionization losses increase with decreasing particle velocity.

An electron with kinetic energy considerably greater than the ionization potential of the atoms of the medium and produced as the result of ionization bremsstrahlung of a particle of charge z is referred to as a δ electron. The maximum energy of the ejected electron is given by the expression

$$E_{\max} = 2mc^2\beta^2/(1-\beta^2),$$

where m is the electron mass, β is the velocity of the incident particle in units of the velocity of light c, and the emission angle of a δ electron with energy E is defined as

$$\cos^2\theta = E/E_{\max}.$$

In the passage of particles through matter with charge Z, atomic number A, and layer thickness x ($g\cdot cm^{-2}$), the total number of δ electrons produced with energies greater than E_1 (MeV) is (Fig. 1)

$$N_\delta = 0.1535\,\frac{z^2Zx}{\beta^2A}\,\frac{1}{E_1}.$$

Most of the electrons are knocked out at an angle of $\pi/2$ and have low energy. We see from Fig. 1 that in the passage of a relativistic proton through 1 cm of argon about 10 electrons are created with energies greater than the ionization potential of the gas, with one in ten having an energy greater than 1 keV. In 5% of the cases the detected particles are δ electrons, whose mean free path in argon is greater than 100 μm, indicating that there is a significant effect on the spatial resolution of the detector. Since there is a nonzero probability for knockout of electrons with energies up to $E_{\max}$, it is possible for some primary electrons to leave the confines of a

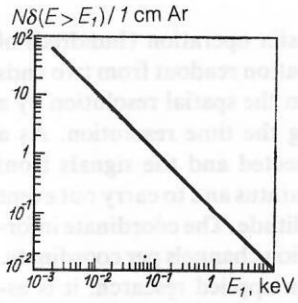

FIG. 1. Number of electrons of energy greater than E_1 knocked out in 1 cm of argon at STP by 10-GeV protons.

thin detector. The dependence of the mean free path of slow electrons in a gas on their energy is shown in Fig. 2.

Electrons with kinetic energy greater than the excitation potential E_{ex} or the ionization potential I of the atoms of the medium can, in turn, excite or ionize the atoms of the medium. In a gaseous medium at STP about three secondary ionization electrons are produced for each primary electron (the number of which per 1 cm of particle path length is n_i). The total number of produced ion pairs, n_T is defined as the ratio of the total particle energy loss in the gas-filled part of the detector to the average energy ω at which the electron pair is produced. Since the total energy loss of a charged particle in a thin layer of matter is the result of a small number of primary interactions (in argon, for example, at STP the average distance between two primary ionization events is 450 μm), its value fluctuates strongly. The probability of producing highly energetic δ electrons causes the ionization distribution to be asymmetric about the most probable value, so that the detector sensitivity must have a large dynamical range. The determination of the average value of the ionization for each particle by means of a large number of independent measurements with about 50% of the largest values discarded forms the basis for particle identification in the region of relativistic growth of the ionization losses when gaseous detectors are used. The distributions of the average ionization (constructed from the values forming the smallest 70% of 192 measurements) are narrow and Gaussian, and the full width at half-max (FWHM) is 8.4%, so that it is possible to distinguish pions from kaons and kaons from protons in the momentum range 5–40 GeV/c.[12] The problems of particle identification have been discussed in detail in Ref. 13, for example, and lie outside the scope of the present study. We note only that in condensed media the density effect, which terminates the growth of the ionization losses with increasing relativistic particle energy, appears earlier than in rarified media.

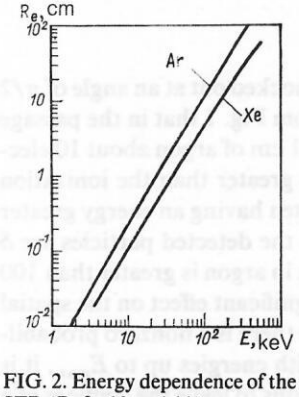

FIG. 2. Energy dependence of the electron mean free path in Ar and Xe at STP (Refs. 10 and 11).

In Table I we give some parameters of the most widely used gases.[3,14–18]

Gaseous coordinate detectors which are sensitive to ultraviolet radiation can be used to identify charged particles with momenta in the range from 1 to hundreds of GeV/c. The identifying elements consist of a gas radiator with a focusing device, in the focal plane of which a coordinate detector is located. When a fast charged particle of velocity β passes through a transparent medium with index of refraction $n>1$, the atoms of the medium become polarized if $\beta n>1$, leading to Vavilov–Čerenkov radiation directed at an angle Θ to the particle trajectory:

$$\Theta = \arccos(\beta n)^{-1}.$$

The number of photons with wavelength in the range from λ_1 to λ_2 emitted by an ultrarelativistic particle with unit charge per path length L is given by the expression

$$N = KL\sin^2\Theta,$$

where

$$K=\frac{2\pi e^2}{\hbar s}\left(\frac{1}{\lambda_2}-\frac{1}{\lambda_1}\right).$$

In the plane normal to the direction of motion of the particle the radiation can be recorded as a ring of definite radius. In the spectral range determined by the quantum efficiency of gaseous coordinate detectors we have the coefficient $K\approx 70$ cm^{-1} (Ref. 19).

X-ray and γ radiation

When a γ flux passes through matter, the intensity of the beam decreases exponentially. Photons are eliminated from the beam as a result of interaction events leading to scattering or absorption. The processes responsible for this are photoabsorption, Rayleigh and Compton scattering, and electron–positron pair production. The latter process can occur for photons with energy above 1.02 MeV. In Fig. 3 we illustrate the contribution of the various processes to the efficiency of the interaction of photons of energy 50–800 keV with lead, which is often used as the external convertor in gaseous detectors. In this energy range the dominant interaction mechanism is the photoelectric effect, while at higher

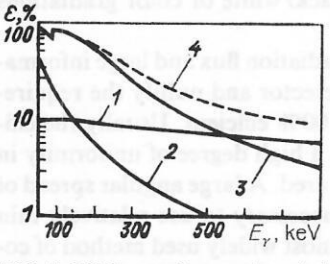

FIG. 3. Efficiency of interaction of photons with energy up to 800 keV in lead of thickness 1 mm: 1—efficiency of Compton scattering; 2—Rayleigh scattering; 3—photoabsorption; 4—total efficiency.

TABLE I. Some parameters of the gases most commonly used in wire coordinate detectors.

Gas	z	A	ρ, mg/cm^3	E_{ex}, eV	I, eV	ω, eV/pair	dE/dx, kev/cm	n_i, con pair/cm	n_T, con pair/cm
He	2	4	0.178	20.9	24.6	41	0.26	3.7	6.3
Ne	10	20.2	0.90	16.6	21.6	36.2	1.17	11	32
Ar	18	39.9	1.78	11.6	15.8	26.2	2.11	22	80.5
Kr	36	83.8	3.74	10.0	14.0	24.0	4.24	41	177
Xe	54	131.3	5.89	8.4	12.1	21.5	6.16	62	286
CO_2	22	44	1.98	10.0	13.8	34.3	2.93	26	85
CH_4	10	16	0.72		13.1	28	1.33	12	48
C_4H_{10}	34	58	2.67		10.6	23	4.5	42	195

energies (in the range 0.5–5 MeV for lead, for example) the Compton effect dominates. Rayleigh scattering, in which the incident photon is deflected without loss of energy, can affect the spatial resolution and is taken into account at low energies. If the gas-filled part of the detector serves as the convertor, Compton scattering becomes the dominant interaction mechanism for photons with energy above 300 or 80 keV, when the gas is Xe or Ar, respectively. In Fig. 4 we show the ratio of the Compton-scattering cross section σ and the photoabsorption cross section τ as a function of the γ energy for several types of matter.

In the photoelectric effect the interaction of a photon of energy E_γ with an atomic electron strips the electron from the atom; here the electron kinetic energy is

$$T_e = E_\gamma - I_i,$$

where I_i is the binding energy of the electron in the ith shell of the atom. The dependence of the electron binding energy on the atomic number of the material is shown in Fig. 5. We note that the cross sections for all the types of interaction mentioned above increase as the charge of the atoms of the medium increases, which determines the choice of convertor.

The vacancies created as a result of the photoelectric effect in the ith shell of the atom are filled after a time of only 10^{-15} sec with electrons from the outer shells. Here a fluorescent photon is emitted with probability ω_i, while in the other cases one of the outer electrons is emitted (an Auger electron).

The fluorescent photon yield for the K shell is[21]

$$\omega_K = P_{K\gamma}/(P_{K\gamma} + P_{Ke}),$$

where $P_{K\gamma}$ is the probability for the atom to deexcite by the emission of a γ quantum P_{Ke} is the corresponding probability for an Auger electron. The energy of the fluorescent photon is determined by the energy difference between the K and L levels:

$$E_{K\gamma} = I_K - I_L,$$

while the energy of the most probable KLL Auger electron is

$$E_e = I_K - 2I_L.$$

The dependence of the probability for, and the energy of, fluorescent radiation on the atomic number of the matter is shown in Fig. 6. Fluorescent emission can lower the spatial and energy resolution of a detector. A fluorescent photon with the average value of the mean free path $\lambda = \mu^{-1}$, where μ is the total attenuation factor, can leave the confines of the detector or can produce a secondary photoelectron from the L shell of the atom far from the primary photoelectron. In Xe at STP, $\lambda \approx 20.7$ cm.

The photoelectrons of soft x-ray radiation are usually emitted at an angle of $\pi/2$ to the photon direction of motion.

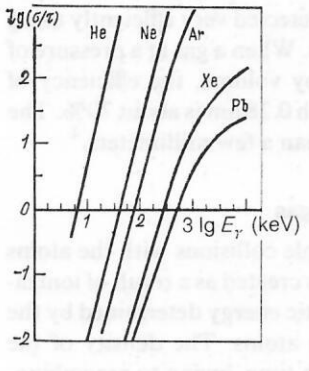

FIG. 4. Ratio of the Compton scattering cross section σ to the photoabsorption cross section τ as a function of the photon energy for several materials.

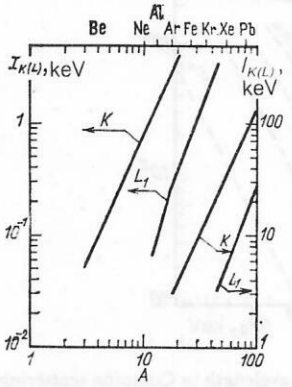

FIG. 5. Dependence of the electron binding energy in the K and L_1 shells of atoms on atomic number (Ref. 20).

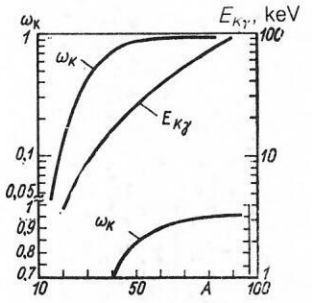

FIG. 6. Dependence of the fluorescent photon yield ω_K and energy $E_{K\gamma}$ on atomic number (Ref. 20).

As the energy increases the photoelectron emission direction approaches the direction of motion of the primary radiation. For example, for photons of energy 1 MeV, 80 keV, and 20 keV the average emission angle is about 10°, 45°, and 65°, respectively.

In the case of Compton scattering the wavelength of the radiation varies from λ_0 to λ, depending on the scattering angle φ, since $\lambda - \lambda_0 = 2\Lambda \sin^2 \varphi/2$, where the Compton wavelength is $\Lambda = 0.002\,42$ nm. Each scattering event is accompanied by the appearance of a recoil electron of kinetic energy (in eV)

$$E_e = \frac{2479.5\Lambda \sin^2 \varphi/2}{\lambda_0 (\lambda_0 + 2\Lambda \sin^2 \varphi/2)},$$

where the wavelength is in nanometers. In Fig. 7 we show the variation of the wavelength of the radiation and the recoil-electron kinetic energy as functions of the energy of the scattered photons for various scattering angles.

High-energy recoil electrons are emitted in the direction of the incident photons. As the energy decreases the angle between the directions of the recoil electron and primary photon emission increases to $\pi/2$. The Compton scattering of the photons occurring before their passage through the working volume of the detector affects the spatial resolution, owing to the change of direction and the energy resolution due to the change in the wavelength. Compton scattering on the atomic electrons of the gas-filled part of the detector can also lead to uncertainty in the coordinate measurements.

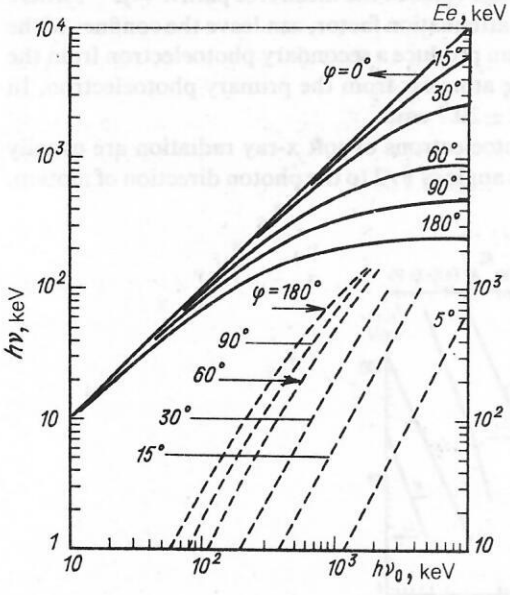

FIG. 7. Dependence of the change of wavelength in Compton scattering on the radiation energy (solid lines) for various scattering angles. Dependences of the recoil electron kinetic energy on the incident photon energy (dashed lines) for various Compton scattering angles.

Neutron detection

The dominant form of neutron interactions with matter is interaction with the nuclei. Neutrons are detected via the ionization due to secondary particles. Fast neutrons are most often detected by detection of the recoil protons. Neutrons of lower energy are detected using the (n,γ), (n,α), or (n,p) reactions. We note that the nuclei formed in radiative capture reactions are usually β^--radioactive.

In the course of their detection, neutrons can interact either with the matter in the gas-filled part of the detector or with the matter serving as the convertor located right next to the detector. In the former case, hydrogeneous compounds, ^{3}He or BF_3, are introduced into the gas-filled part of the detector. Usually, CH_2, ^{6}LiF, ^{10}B, Gd, or Dy are used as external convertors; materials which selectively capture neutrons of resonance energies also might be used.

In the detection of thermal neutrons via the reaction B(n,α)Li usually the coordinates of the stopping points of α particles of energy 1.5 MeV, which are a considerable distance from the neutron conversion points, are determined. Here the spatial resolution is no better than 2–3 mm (Ref. 22). If the specific ionization losses of the secondary radiation are sufficiently large, it is possible to use low-pressure gaseous detectors with so-called focusing properties, allowing the accuracy to be improved to a fraction of a millimeter.[23,24] While the mean free path of an α particle of energy 1.5 MeV in argon at STP is about 1 cm, in boron it is about 4 μm, which determines the effective thickness of the converter. An estimate of the efficiency of the α-particle yield from a converter of thickness 0.4 mg·cm^{-2} with an enrichment of ^{10}B of up to 90% showed that the expected efficiency of thermal-neutron detection by a gaseous detector with a ^{10}B converter is about 1% (Ref. 25). The secondary-particle yield is doubled if convertors are put on both sides of the detector.

Thermal neutrons can be detected very efficiently using high-pressure gaseous detectors. When a gas at a pressure of 1013 kPa contains 60% ^{3}He by volume, the efficiency of detecting neutrons of wavelength 0.28 nm is about 70%. The spatial resolution is no better than a few millimeters.[4]

Electron diffusion and drift in a gas

When they undergo multiple collisions with the atoms of the gas, the electrons and ions created as a result of ionization lose a fraction of their kinetic energy determined by the average thermal energy of the atoms. The density of the charge produced decreases with time, owing to recombination and electron loss via capture by electron-deficient molecules. The electron-capture probability is characterized by

the sticking probability h, which is the ratio of the cross section for negative-ion production to the total cross section for electron interactions with atoms. For the inert gases H_2 and N_2, $1/h \sim \infty$, while for CO_2, for example, $1/h \sim 1.6 \times 10^8$ (Ref. 26).

When an electric field is present, the electron cloud is shifted a distance x toward the anode during a time t. Here the electron coordinates acquire a spread with rms deviation

$$\sigma_x^2 = 2Dt = 2\varepsilon_K x/eE,$$

where D is the diffusion coefficient and ϵ_K is the characteristic electron energy ($\epsilon_K = kT$ for an ideal gas). In strong electric fields ϵ_K can grow significantly for some gases, while in others (for example, CO_2) the electrons remain thermal even in strong fields. In an electric field such that $E/p > 10^{-3}$ V/(cm·mm Hg)[a] the diffusion along the direction of the field D_L is different from that in the perpendicular direction D_T. For example, in helium with hydrogen, argon, and xenon the ratio D_T/D_L is roughly 2, 7, and 10, respectively.[27] Electron diffusion affects the maximum accuracy of the detector. In the detection of the most energetic k electrons of n primary electrons in a drift chamber, for example, the coordinate accuracy is given by[18]

$$\sigma_k = \left(\frac{1}{2\ln n}\sum_{m=k}^{n}\frac{1}{m^2}\right)^{1/2}\sigma_x,$$

where σ_x is related to the electric field strength and the gas pressure p as

$$\sigma_x = f(E/p)\,(x/p)^{1/2}$$

The average velocity of charges in an electric field moving toward the corresponding electrode is referred to as the drift velocity W. If the average energy of ions in an electric field is practically unchanged, the electrons acquire an energy whose maximum value is determined by the lower energy levels of the atoms of the gas. The energy acquired by the electrons can be decreased by adding a gas of high molecular

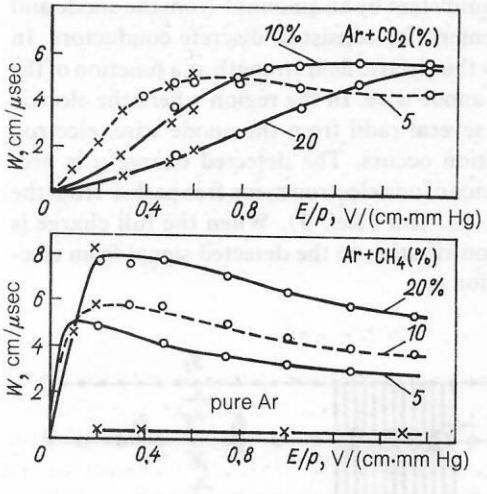

FIG. 8. Dependence of the electron drift velocity in a mixture of Ar and CO_2 (upper figure) and in Ar and CH_4 (lower figure); O are the results of Ref. 28, and × are those of Ref. 29.

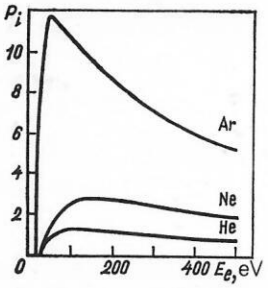

FIG. 9. Dependence of the ionization probability of several inert gases on the electron energy (Ref. 29).

weight with many low-lying excited states to a pure gas with a high first excited state. The cross section for electron–atom interactions decreases and the mean free path between collisions increases, causing the drift velocity to increase. In Fig. 8 we show the dependence of W on the ratio E/p for several mixtures. The analogous dependences for various mixtures of gases are given in Ref. 30.

Inelastic collisions of electrons with atoms

If the energy acquired by the electrons between two collisions in a strong electric field is greater than or equal to the energy of an excited state, the atom is excited. In molecular gases the electrons excite the vibrational levels of the ground state, and the energy that they lose is considerably less than in the case of monatomic gases. If between two collisions an electron acquires an energy greater than the ionization potential of the atoms of the gas, ionization occurs. In Fig. 9 we show the dependence of the ionization probability of several inert gases on the electron energy. At high values of E/p, beginning with some value of the field strength, the ionization can become shower-like. If the initial number of electrons is n_0, the total number of shower electrons at the end of a path of length x in a uniform field is $n = n_0 e^{\alpha x}$, where the first Townsend coefficient α determines the multiplication factor of a primary electron over a path of length 1 cm in the direction of the field. The gas amplification is $e^{\alpha x}$. The dependence of α on the electric field for inert gases is shown in Fig. 10. The energy acquired by an electron between two collisions is

$$T_e = (E/p)\,e\,\frac{1}{\alpha/p},$$

where e is the electron charge. Shower development occurs

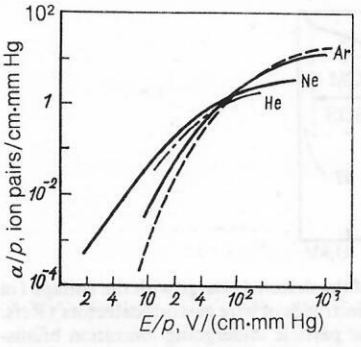

FIG. 10. The first Townsend coefficient for several inert gases (Ref. 29).

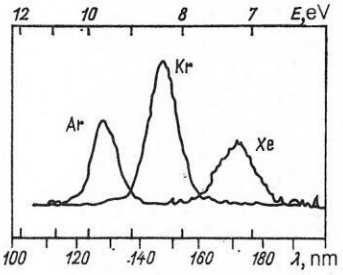

FIG. 11. Emission spectra of several inert gases (Ref. 31).

efficiently in a field for $E/p > 100$ V/(cm·mm Hg).

The addition of, for example, Ar to Ne leads to a large increase in α due to the so-called Penning effect. This goes as follows. As a result of inelastic collisions between electrons and atoms of the main component of the gas A, the atoms are excited and then deexcite via photon emission $A^+ \rightarrow h\nu + A$. The emission spectra of several inert gases are shown in Fig. 11. If the excitation potential of the atoms A is higher than the ionization potential of the atoms of the admixed gas B, ionization occurs: $h\nu + B \rightarrow B^+ + e$. Multistep shower chambers at normal pressure work in a similar manner.

The charge-collection mechanism in gaseous detectors

The number of ion pairs collected at the electrodes of a detector, that is, the size of the detected signal, can vary, depending on the strength of the electric field. This is illustrated in Fig. 12, which can be divided into six parts. In region I charge accumulation is hindered by ion recombination. When the field strength is increased, the drift velocity increases and the recombination probability decreases. In the case of a mixture of argon with about 10% gases of high molecular weight the recombination process is negligible for $E/p > 0.65$ V/(cm·mm Hg) (Ref. 32). Complete charge accumulation occurs in region II of Fig. 12. When the field strength is increased further, we enter the proportional regime, region III. At high field strengths electron showers are produced and move to the anode with velocity 2×10^7 cm/sec (Ref. 26) in the form of an electron cloud leaving positive ions behind. The change of the electric field due to the space charge corresponding to the positive ions causes the gas amplification coefficient M to depend on the primary ionization at large values of M. The energy resolution of the

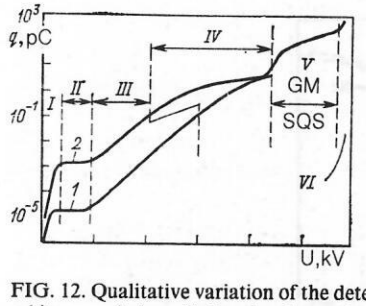

FIG. 12. Qualitative variation of the detected charge with the voltage (in arbitrary units) applied to the electrodes of wire gaseous detectors (Refs. 32 and 35): 1—for a relativistic particle undergoing ionization bremsstrahlung in 1 cm of argon at STP; 2—for the case of large ionization losses.

detector begins to deteriorate in this regime of limited proportionality (region IV). The value of the gas amplification coefficient M_k corresponding to the onset of this regime is

$$M_k = Q_k/E,$$

where E is the ionization loss per unit length of a discrete element of a wire detector. The coefficient Q_k for such detectors (MWPCs) has been determined in Ref. 32 and is 3×10^7 eV. In the case of relativistic-particle detection by a detector of thickness 1 cm the amplification coefficient M_k for Ne, Ar, and Xe is about 2×10^4, 10^4, and 5×10^3, respectively.

Further increase of the field strength leads to the Geiger–Mueller (GM) regime or, when certain conditions are satisfied, to the SQS regime, region V. In the GM regime the dead time of the detector is $\sim 500\,\mu$sec per discrete element. When the concentration of gas with high molecular weight is sufficiently large, the shower propagation probability is decreased because of photoionization and the development of primary showers leads to the formation of a streamer which propagates along the electric field lines. The streamer stops growing when it reaches the weak-field region. In this (the SQS) regime a discrete element of the detector has a dead zone of about 30–90 μsec·cm. The review of Ref. 33 is devoted to detectors operating in the SQS regime. We note that an SQS detector can operate in the so-called two-streamer regime, where two independent streamers develop from opposite sides of the anode wire. This causes the signals to have different amplitudes when radiation significantly differing in mass and charge is detected.[34]

Region VI corresponds to electrical breakdown of the gas gap.

3. COORDINATE DETECTORS

Multiwire proportional chambers (MWPC)

Operating principles. An MWPC can be viewed as a set of cylindrical counters located in a single gas-filled volume. As a rule, they contain three electrodes (Fig. 13). The inner one is the anode and usually consists of wires of diameter $d = 20\,\mu$m with pitch $s = 2$ mm. The outer electrode, the cathodes, are equidistant by an amount l from the anode and can be solid elements or consist of discrete conductors. In Fig. 14 we show the electric field strength as a function of the distance to the anode wire. In the region where the electric field is strong, several radii from the anode wire, electron shower production occurs. The detected charge q is produced at a distance of one electron mean free path λ from the wire; in argon $\lambda \approx 1\,\mu$m (Ref. 3). When the full charge is collected, the contribution to the detected signal from electron accumulation is

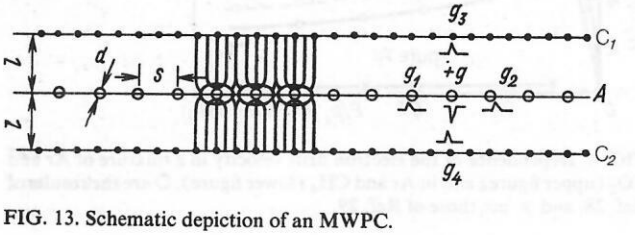

FIG. 13. Schematic depiction of an MWPC.

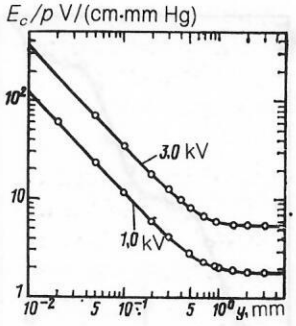

FIG. 14. Dependence of the electric field strength on the distance from the center of the anode wire in the direction of the cathodes for various voltages in an MWPC. The MWPC parameters are $l = 5$ mm, $s = 2$ mm, and $d = 20\,\mu$m.

$$V^- = -\frac{q}{2\pi\varepsilon_0 l}\ln\frac{d+2\lambda}{d},$$

while that from the motion of positive ions is

$$V^+ = -\frac{q}{2\pi\varepsilon_0 l}\ln\frac{2l}{d+2\lambda}.$$

For $l = 5$ mm and $d = 20\ \mu$m we have the ratio $V^-/V^+ = 0.015$. Therefore, the detected pulse is determined mainly by the removal of positive ions from the region closest to the wire.

The time for the full accumulation of the charge is determined by the mobility μ^+ of positive ions in the gas and can be estimated to be

$$t = (l/\mu^+)\,(E/p)^{-1}.$$

Since $\mu^+ \simeq 1.5$ cm$^2\cdot$V$^{-1}\cdot$sec^{-1} (Ref. 36), for an MWPC with $l = 5$ mm and $E/p = 1.5$ kV/(cm·mm Hg), $t \simeq 0.2$ msec. Analysis of the signal guided to the anode wire indicates that 8% of the total signal reaches the wire in the first 10 nsec, while about 14% of it reaches it in the first 100 nsec (Ref. 37). When photons are detected, the primary ionization is localized in a small region and the time for the collection of charge from the showers of all the primary electrons is small. When charged radiation is detected, all of the primary electrons are collected during 100–150 nsec, taking 20 nsec to travel 1 mm. This determines the constant of differentiation in the accumulation of charge of the fast component.

The signal of negative polarity recorded from the anode wire is determined by the charge q. Here signals of positive polarity determined by the charges q_j (Fig. 13), where $-q = \Sigma q_j$, are guided on the adjacent wires and on the cathodes. In Fig. 15 we show the dependence of the signal amplitudes at the exit of the linear amplifier when the signals are taken from the anode plane (all the wires are joined together) and from the discrete elements of the cathodes. When the anode wires are joined together, the capacitance connected to the input of the amplifier is increased, which for this particular MWPC leads to a factor of 8 reduction of the anode signals compared to the case of discrete readout. When this is taken into account, it follows from Fig. 15 that $\sim 0.33q$ is guided to the cathode C_1, $\sim 0.25q$ to C_2, and $\sim 0.2q$ is on the neighboring anode wires. Therefore, for the

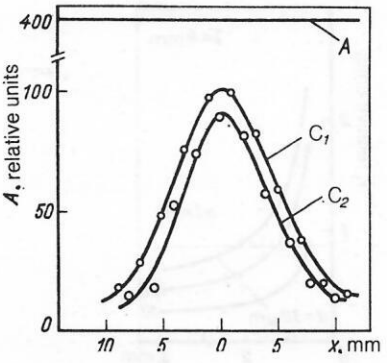

FIG. 15. Dependence of the amplitude of the anode signal (A) and of the signals directed to discrete elements of the cathodes on their distance from the center of the shower. The MWPC size is 250×250 mm^2, $l = 3$ mm, $s = 2$ mm, $d = 20\,\mu$m, and the cathodes C_1 and C_2 have 1-mm pitch.

case of discrete readout from the anode and from the cathodes, the sensitivity of the cathode amplifiers should exceed that of the anode amplifiers by about a factor of 30. The dependences that we give were obtained using a ^{55}Fe source, and the photon conversion occurred mainly near the cathode C_1. A slight difference between the signals from the cathodes C_1 and C_2 is observed, owing to the angular localization of the showers near the anode wires.[36,38]

The efficiency. For a given amplifier sensitivity the MWPC efficiency is determined by the type of gas used, the applied potential U, and the geometrical parameters of the detector. A large number of gas mixtures are known which ensure a charged-radiation detection efficiency of close to 100%. When there are no special requirements such as obtaining the maximum time resolution or gas amplification or requiring that the gas filling the detector have a large effective density, the most suitable commercial two-component mixtures are Ar with 20%–30% CH_4 or CO_2. When the chamber is flushed with the gas mixture, a small fraction of alcohol vapor is introduced, which increases the efficiency plateau by about 40% (Ref. 39). The alcohol molecules inhibit the photoelectric effect at the cathodes and the secondary electron production occurring when the positive ions approach the cathode. In some cases, particularly for large MWPC, which are difficult to prepare with the necessary accuracy, it is better to use gas mixtures containing electron-deficient additives, for example, the "magic" mixture consisting of argon, isobutane (23%), freon-13B1 (0.2%), and methylal (4%) (Ref. 40). In these mixtures the gas amplification coefficients are high and spontaneous electrical breakdown does not occur, so that a sufficiently large efficiency plateau is obtained. For an MWPC with pitch $s = 1$ mm it has been proposed that a mixture of argon with 14% $C_3H_8O_2$ and 50% CO_2 be used to ensure high efficiency and stable operation.[41]

In Fig. 16 we show the variation of the voltage as a function of the anode wire pitch for fixed electrical field strength at the surface of anode wires of various diameters. The voltage at which electrical breakdown occurs in accordance with the Raether condition $\alpha l = 20$ (Ref. 26) is marked. A decrease of the diameter of the anode wires low-

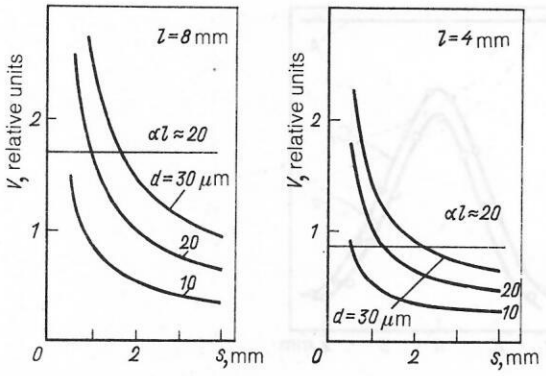

FIG. 16. Dependence of the voltage on the anode pitch for MWPC with various electrode spacings l and various anode wire diameters.

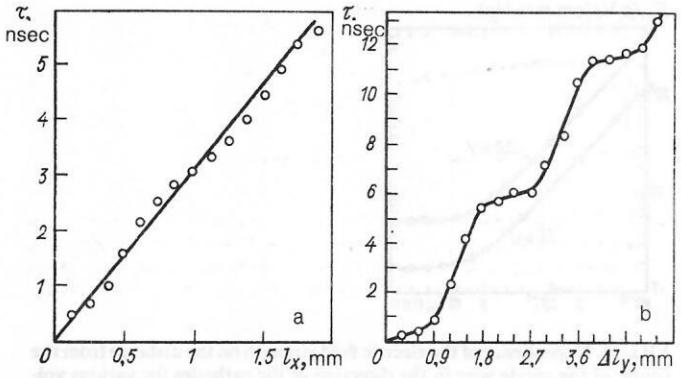

FIG. 17. Dependence of the delay of a coordinate signal read out using a cathode delay line on the displacement of a photon beam of diameter 0.15 mm (a characterization of the detector linearity) (Ref. 49) when the beam is displaced along the anode wires (a) or perpendicular to the anode wires (b).

ers the required values of the voltage and makes it possible to obtain a higher gas amplification. However, electrostatic difficulties restrict the use of wires of small diameter.[42] As the spacing between the electrodes decreases the capabilities of the MWPC deteriorate somewhat. For example, when l is changed from 8 to 4 mm, the minimum possible value of s for wires of a given diameter increases by 20%. We note that a 1% variation of the diameter of the anode wires changes the gas amplification coefficient by 10%–15% (Ref. 43).

The *temporal resolution* of an MWPC is defined as the full width at half-max (FWHM) of the curve of delayed coincidences between the signals from the chamber and the resolving signal at the electronic detection apparatus. Its value is determined both by the duration of the resolving signal and by the width of the time distribution of the signals from the MWPC. In the detection of charged radiation with 99% efficiency the time resolution is usually no worse than 40–50 nsec. The FWHM of the time spectrum of the distribution of signals from the MWPC and at the level where 99% of the events are detected is 10 and 30 nsec, respectively, for a mixture of Ar and CO_2.[44,45] For a mixture of Ar and isobutane these times are increased to 12 and 50 nsec. The highest resolution is obtained for mixtures based on neon; for example, for Ne with 20% CO_2, 8% Ar, and 3.5% C_2H_5OH these values are 8 and 23 nsec, respectively.[46]

In the case of analog readout of information by means of delay lines (DL), the time resolution of the chamber for the anode and cathode signals must be distinguished in some cases. Whereas the time resolution for anode signals is usually about 50 nsec, that for cathode signals is the same as the dead time ($\tau_d \approx \tau_1 L$, where τ_1 is the linear delay of the lines and L is the linear dimension of the detector). In fact, in the detection of two events which are simultaneous or separated by a time smaller than τ_d, the uncertainty in the determination of the coordinates of each particle cannot be eliminated. The time resolution of an MWPC with analog readout is usually 0.5–1 μsec. The good time resolution for the anode signals is used to exclude background events by analysis of their coincidences with fast monitor signals.

Spatial resolution. The uncertainty in the determination of the coordinates of particles detected by MWPCs with digital readout corresponds to the distance between the anode wires and is $\pm s/2$. As for any rectangular distribution, the rms deviation is $\sigma = s/\sqrt{12}$. For MWPCs with anode wire pitch equal to 2 mm, the resolution is $\sigma = 0.56$ mm (Ref. 47). Decreasing the distance between the anode wires improves both the spatial and the time resolution and raises the efficiency of the detector when used in intense particle beams. However, for this it is necessary either to raise the high voltage in order to ensure the necessary gas amplification or to increase the sensitivity of the amplifiers. These requirements can be weakened somewhat by decreasing the diameter of the anode wires. There are quite a few studies on the use of MWPCs with anode wire pitch equal to 1 mm. For example, such MWPCs have been used successfully for the diagnostics of a separated antideuteron beam at IHEP.[41] A vertex detector has been constructed using a set of 18 MWPCs with anode pitch 0.5 mm, the individual chambers being shifted relative to each other by an amount $s/2$. The resulting resolution is $\sigma = 80\,\mu$m (Ref. 48).

The value of s does not restrict the spatial resolution in the case of cathode readout from an electrode whose wires are perpendicular to the anode. The dependence of the delay of the centroid of the cathode signal on the shift of the x-ray beam along the anode wires [Fig. 17(a)] shows that the MWPC is equally accurate in this coordinate and that the differential nonlinearity is about $\pm 60\,\mu$m and periodic in nature. The readout was done by means of DL. Such modulations can be manifested as a distortion of the shape of the signals from the DL (with period related to the pitch of the lines) and as a nonuniformity of the field near the cathode wires.[50] The accuracy of measurement of the second coordinate [Fig. 17(b)] obtained from an electrode whose discrete elements are parallel to the anode elements is related to the pitch s. Since the shower that develops near the anode wire does not envelop it completely but rather is spatially oriented, the centroid of the directed charge is shifted by an amount related to the distance of the conversion point from the anode wire. The observed dependence of the delay of the coordinate signals on the shift of the γ beam [Fig. 17(b)] indicates that better resolution can be obtained than in the case of a rectangular distribution.

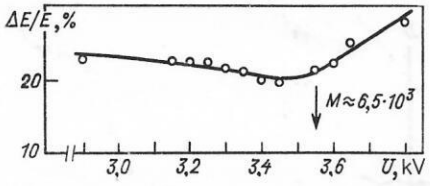

FIG. 18. Dependence of the MWPC energy resolution on the voltage across the chamber. Photons of energy 5.9 keV are detected (Ref. 32). The arrow indicates the voltage and the value of the gas amplification at which the detector begins to operate in the regime of limited proportionality.

When the coordinate readout is done by DL, the spatial resolution of the detector can be limited by the intrinsic resolution of the electronics[51,52]: $\sigma_{el} = A_n t_f / A_s \tau_l$, where A_s is the amplitude of the detected signal, A_n is the rms amplitude of the noise, and t_f is the signal front (usually 50–100 nsec). In practice, lines with $\tau_l = 1$–10 nsec/mm are used, and to ensure good resolution the signal-to-noise ratio should be at least 50. The resolution $\sigma = 100\,\mu$m has been obtained in the detection of 5.9-keV photons.[51] A two-coordinate readout is possible by separation of the charge from special electrodes, so that the X and Y coordinates are encoded in the charge ratio.[53–55] The electrodes are printed on glass laminate in the form of a series of wedges and strips whose area depends linearly on the coordinates. Here, in contrast to the case of resistive readout, the accuracy is limited only by the shower size. For MWPCs with length dimensions of several meters it is believed that a spatial resolution of about 0.1% of the length of the anode wires can easily be attained by this method.[55]

Energy resolution. The charging ability. The dependence of the energy resolution of an MWPC on the voltage across the chamber is shown in Fig. 18. In the region of proportional amplification the energy resolution is about 20% and worsens when the MWPC is operated in the limited-proportionality regime. The gas amplification of the chamber usually lies in the range 10^5–10^6, and the energy resolution is generally no better than 30%. If the spread of values of the coefficient M over the entire area of the MWPC is not to exceed 35%, the accuracy of the pitch of the anode plane should be 1%.[56]

By analogy with proportional counters, the pulse input to the amplifier, that is, the sensitivity, can be estimated from the expression

$$V = k\frac{MEe}{C\omega}, \qquad (T)$$

where E is the energy of the ionization losses and C is the capacitance of the input circuit and the discrete element of the detector to which the amplifier is connected. The coefficient k is taken to be 0.5.[57] An important characteristic of the MWPC as a high-speed detector is its charging ability, defined as the maximum particle flux per unit area per unit time which leaves the characteristics unchanged. An important limit on the charging ability of an MWPC is the space charge of the positive ions, which affects the gas amplification coefficient. In Fig. 19 we show the variation of the anode signals as a function of the intensity of an 8-keV photon flux.

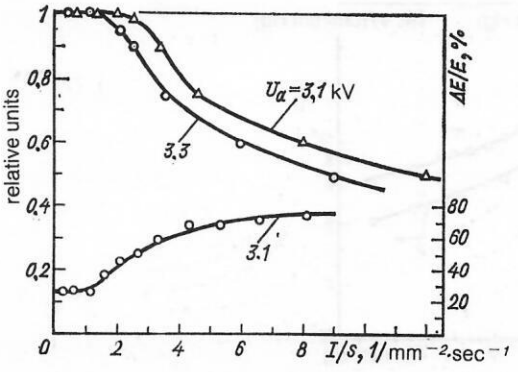

FIG. 19. Dependence of the values of the average amplitude of the signals from an MWPC anode wire on the unit amount of charge loading for various voltages U_a across the chamber. The lower curve shows the variation of the energy resolution with the charge loading. The radiation consists of 8-keV photons. The gas is xenon plus 20% methane and 3% ethyl alcohol. The dimensions of the MWPC are 350×350 mm^2.

All of the anode wires are joined together, which increases C, and the coordinate information is read out from the cathodes by means of DL. We see that for photon-flux intensities greater than 1.5×10^3 mm$^{-2}\cdot$sec^{-1} the space charge decreases the signal amplitude and worsens the energy resolution.

The speed of response of an MWPC can be increased as follows: by decreasing the pitch s and thereby the charge loading per wire, by decreasing the gap distance l and thereby the effect of the space charge and the signal "tails" due to delayed electrons, by decreasing the diameter of the anode wires to improve the time resolution for the anode signals and decrease the effect of the space charge, and by using low-noise amplifiers so that it is possible to work with a lower gas amplification.

Low-pressure MWPCs. The properties of chambers filled with hydrocarbon gases at low pressure have been investigated for the purpose of detecting recoil nuclei in experiments on π and p scattering on He.[58,59] It has been shown that such chambers have good space-time characteristics. A spatial resolution $\sigma = 40\,\mu$m has been obtained in the detection of 5.5-MeV α particles using a chamber filled with heptane at a pressure of 77 mm Hg (Ref. 59). The time resolution of an MWPC filled with heptane or isobutane at a pressure of several millimeters of Hg was found to be 2.5 nsec (FWHM), while in the case of ethylene at 5 mm Hg it was 0.8 nsec (Ref. 60). Later these detectors were investigated and developed further, mainly for the detection of fission fragments of nuclear reactions in heavy-ion physics. Their typical parameters are as follows: a sensitive area of up to 10×10 cm^2, time resolution of 0.2–0.5 nsec (FWHM), spatial resolution of 0.5–1 mm (FWHM), and average matter content of about 600 μg/cm^2 (Ref. 61).

The special features of low-pressure MWPC are the rapid collection of the ionization products and the additional gas amplification due to electron collisions in the region between the anode and the cathode. It follows from Fig. 20 that for isobutane gas at a pressure of less than 15 mm Hg the strength of the uniform electric field in the MWPC can

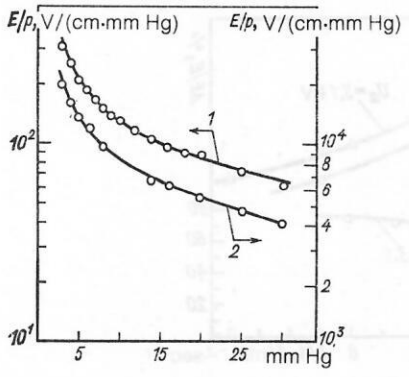

FIG. 20. Dependence of the maximum value of the field strength in the region of uniform electric field (curve 1) and at the surface of the anode wires (curve 2) on the isobutane pressure. The MWPC parameters are $l = 4$ mm, $s = 2$ mm, and $d = 20\,\mu$m (Ref. 62).

exceed 100 V/(cm·mm Hg), with additional amplification possible. In order to increase the efficiency plateau and improve the signal-to-noise ratio in the detection of light nuclear fragments of relatively low energy, an additional drift gap (DG) can be introduced. If the field in a DG of 4 mm is sufficiently uniform and isobutane at a pressure of 5 mm Hg is used, the gas amplification of the detector can be increased by an additional factor of almost 100. This allows the detection of particles with total ionization loss greater than 4 keV. For 5-MeV α particles the spatial resolution is about 0.1 mm and the time resolution is better than 3 nsec (Ref. 62).

Multiwire proportional chambers filled with a mixture of isobutane gas at 3 mm Hg and TMAE gas at a partial pressure of 0.28 mm Hg in conjunction with BaF_2 scintillators are used in electromagnetic calorimetry. A chamber filled with such a gas mixture is sensitive to ultraviolet radiation, and the coordinate information is read out from the cathodes and the anodes. We note that BaF_2 is not hygroscopic, it has a high density ($\rho = 4.9$ g/cm^3), its radiation length is 2.1 cm, and it is 500 times faster than NaI(T1) or BGO. The calorimeter contains 14 detector modules (19.3 radiation lengths), and for electrons of energy 0.1–0.2 GeV it ensures an energy resolution of $\sigma/E = 2.5E^{1/2}\%$, where E is in GeV (Ref. 63).

Drift chambers

The coordinates of particles produced by ionization of the gas in a drift chamber are determined by measuring the drift time of electrons in a uniform electric field. The operation of such detectors has been described in detail in Refs. 3 and 5. We note that the ability of DC to operate in a wide range of gas pressures significantly increases their region of applicability. For example, low-pressure DC are used in heavy-ion physics,[60] and at high energies they have been used successfully to study the radiation of relativistic particles in monocrystals, where high resolution in the scattering angle and low bremsstrahlung background are required.[64] These detectors can also be used for neutron radiography.[65]

The operation of a DC is affected by a number of factors which can change the electron drift velocity: errors introduced in the construction of the detector which lead to non-

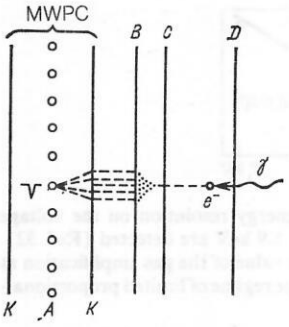

FIG. 21. Schematic depiction of a multistep shower chamber.

uniformities in the electric field and instability in the magnitude and direction of the field and to errors in the composition of the gas mixture. Among the external factors which tend to destabilize the operation of a DC are the atmospheric pressure, the temperature, and external magnetic fields. For example, a 1% variation in the composition of the gas leads to a 0.12% change in the drift velocity,[66] while a 1 V variation of the voltage leads to a 0.06% change of the velocity.[64] Nevertheless, when certain conditions are met the drift velocity can be stabilized to within 0.5% over prolonged operation. The maximum accuracy of a such DC system is about $\sigma = 100\,\mu$m.

Allison *et al.*[67] have demonstrated the operation of DC without field-shaping electrodes. Here a voltage is supplied to the signal wires (the anodes) and the cathodes, which are located at the ends of the drift gaps, are grounded. The walls shielding the sensitive part of the detector are made of a good insulator. The external metallized surface of the walls is grounded. The accumulation of positive ions on the inner surface of the walls automatically creates a uniform electric field. These detectors are extremely simple to prepare[68] and can operate at particle fluxes of up to 10^5 sec^{-1} per wire.[69] Highly efficient collection of ionization electrons over a distance of more than 1 mm is possible even when the trajectories are curved by using plastic tubes with a spatial resolution of about 2 mm (Ref. 70).

Multistep shower chambers (MSSC)

The operation of MSSC at normal pressure is based on obtaining additional gas amplification in the strong uniform electric field of the preliminary-amplification gap (BC in Fig. 21) by filling the detector with an inert gas with a 1%–3% admixture of gas with high molecular weight. The atoms of the principal component of the gas mixture are ionized and excited by electron collisions. De-excitation occurs by the emission of photons which ionize the molecules of the admixed gas if the photon energy is greater than the ionization potential of the molecules. In Table II (Refs. 7, 31, 71, and 72) we give the values of I and the saturated vapor pressures p_s of various gases at the temperatures 0 ° and 20 °C (denoted by the star *) used as the additive. An MSSC consists of an ordinary MWPC with a series of auxiliary electrode grids B, C, and D across which the required electric potentials are supplied. Interactions between photons and

TABLE II. Values of the ionization potentials of several organic compounds used as the addition to the gas. The saturated vapor pressure is given for liquids.

Compound	Methane (CH_4)	Isopropylene alcohol (C_3H_8O)	n-heptane (C_7H_{16})	Acetone (C_3H_6O)	TEA [$(C_2H_5)_3$]	Ethylferrocene	TMAE
I, eV	12.6	10.2	10.1	9.7	7.5	6.0	5.36
p_s, mm Hg	—	8.5	11.5	67	20	<1 *	0.35 *

gas atoms in the conversion gap CD produce electrons which drift to the preliminary-amplification gap, leading to the appearance of a charge q in that region. The motion of the charge in the strong uniform field leads to a current given by

$$\frac{dQ}{dt} = \frac{qW}{l} e^{\alpha W t},$$

where l is the gap width. From this it follows that the charge Q accumulated at electrode B during time $t = l/W$ is

$$Q = q\,(e^{\alpha l} - 1)/\alpha l.$$

The drift gap BK serves to transfer the charge to the sensitive region of the MWPC. The detected charge is $Q^* = fG_1G_2q$, where G_1 is the preliminary amplification of the gap BC and G_2 is the gas amplification of the MWPC. The coefficient f determines the fraction of charge that has passed through electrode B to the gap BK. For $E_2 < 0.2E_1$, where E_1 and E_2 are the field strengths in the gaps BC and BK, respectively, the coefficient is $f \sim E_2/E_1$ (Ref. 73).

In Fig. 22 we show typical dependences of G_1 on the field strength in the preliminary-amplification gap. The relation between the field strength in this gap and the voltage across the MWPC is shown in Fig. 23, where the dependences correspond to a fixed value of the gas-amplification coefficient of the detector M. The preliminary amplification of the detector reaches 10^4, which makes it possible to lower the voltage across the MWPC considerably. An additional enhancement of up to 5×10^3 is usually ensured; at higher values sparking across the gap BC occurs occasionally. The stability of operation of the MSSC is to a significant degree determined by the stability of the partial pressure p of the gap mixture. For example, for a mixture of argon and acetone $M \sim p^{-10}$ (Ref. 74). The gas control system must be thermally stabilized, and in the case of MSSC with mylar entrance windows it is necessary to stabilize the gas channel rate.

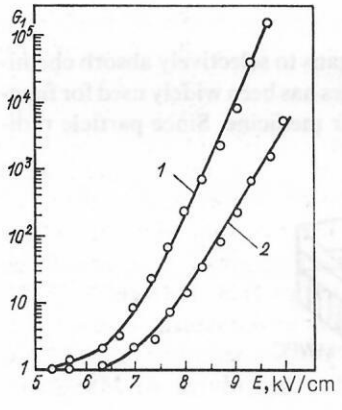

FIG. 22. Dependence of the preliminary-amplification coefficient on the field strength: curve 1—argon with 1.6% acetone; curve 2—argon with 3% acetone.

The space-time characteristics of MSSC at normal pressure are the same as those of MWPC. In the case of charged radiation entering the preliminary-amplification gap at large angles, the strongest signals are from the primary electrons produced at the beginning of the gap (there is no conversion gap). The coordinates of points on particle tracks in the plane C are determined, that is, the detector possesses "focusing" properties.

When a gas of low ionization potential (5–7 eV) is introduced into the gas mixture, the MSSC can detect ultraviolet radiation and can be used, for example, in Čerenkov-radiation detectors[75] and for plasma diagnostics.[72] A detector of area 20×20 cm^2 with gas content 90% He, 7.5% CH_4, and 2.5% TEA localizes single photoelectrons with an accuracy of, for example, 0.9 mm (FWHM) and has a gas amplification of about 10^6 (Ref. 76).

The possibilities offered by low-pressure MSSC are discussed in Refs. 77 and 78. The detector is filled with a pure hydrocarbon mixture, for example, methane or isobutane, at a pressure of several millimeters of Hg. A field $E/p > 100$ V/(cm·mm Hg) is created in the preliminary-amplification gap, and in this case showers can be produced by electron collisions. The shower electrons pass through the drift gap and into the MWPC, where further amplification occurs via a two-stage process: first in the uniform field via electron collisions, then at the anode wires. At low pressures the transverse dimension of the showers leaving the gap BC is

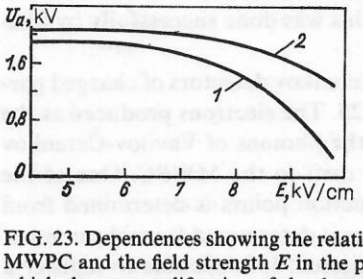

FIG. 23. Dependences showing the relation between the voltage U_a in an MWPC and the field strength E in the preliminary-amplification gap at which the gas amplification of the detector is constant: curve 1—argon with 1.6% acetone; 2—argon with 3% acetone. The amplitude of the signals at the output of the linear amplifier is 200 mV.

about 1 mm (FWHM) (Ref. 79). Diffusion of the electrons in the drift gap increases this value, thereby ensuring that the detector is equally accurate at measuring both coordinates and also decreasing the unit charge density so that a larger amplification can be obtained. A large amplification ensures a good signal-to-noise ratio, that is, good spatial resolution. Low-pressure MSSC possess the following properties:

1. The time resolution is a fraction of a nanosecond.
2. The gas amplification in isobutane at 6–20 mm Hg reaches 10^7.
3. The speed of response is increased by the diminishment of the role of the positive-ion space charge owing to the high ion drift velocity.
4. They are not very sensitive to relativistic particles, but still they are suitable for detecting radiation with ionization losses exceeding 150 eV (Ref. 78).
5. They can detect single photoelectrons with close to 100% efficiency.[80]
6. Both coordinates are measured with equal accuracy, and the spatial resolution is better than 0.2 mm (FWHM).[80]
7. The detector can have a fairly large area—for example, that in Ref. 78 has area 24×18 cm.

Time-projection detectors (TPD)

The operation of TPD is based on the electronic projection of the tracks of ionizing particles from the drift chamber onto the sensitive electrode of the coordinate detector. The following quantities can be measured: the track distribution of the particle ionization, the mean free path when particles are stopped inside the drift gap (the X coordinate), the Y coordinate of the points on a track by one of the analog methods of coordinate cathode readout, and the electron drift time in the gap, that is, the Z coordinates of points on a track. Therefore, it is possible to reconstruct the spatial picture of the motion of charged particles and to measure the ionization density on a track, so that such detectors can be used to identify slow nuclear fragments in a wide range of mass and charge. A detector with a sensitive volume of $100\times 40\times 12$ cm^3 (the length, width, and size of the drift gap, respectively) using argon with a 10% admixture of methane reliably identifies hydrogen and helium isotopes. The event mass distribution (Fig. 24) indicates that the resolution is 10% (FWHM) for protons and 6% for helium. Such a detector is a good instrument for the identification and spectrometry of slow particles and, when filled with helium gas, it can serve as a polarimeter for protons and deuterons.[81]

Allison[82] proposed that such detectors be used to identify relativistic particles; this was done successfully by Shapiro *et al.*[12]

The use of TPD for Čerenkov detectors of charged particles is illustrated in Fig. 25. The electrons produced as the result of the detection of the photons of Vavilov-Čerenkov radiation in the drift gap drift to the MWPC. One of the coordinates of their production points is determined from the drift time, and the other is determined from the number of the wire which was triggered. It is possible to register a larger number of electrons of the Čerenkov ring by a small number of measuring channels without any spatial uncertainty. The identifying element consists of a gaseous radiator (C_4H_{10} or Ar) separated by a quartz window from a coordinate detector filled with a mixture of gases, for example, 80% CH_4, 20% C_4H_{10}, and TMAE. Such setups have been constructed for the OMEGA spectrometer[83] at CERN and for the DELPHI installation.[84]

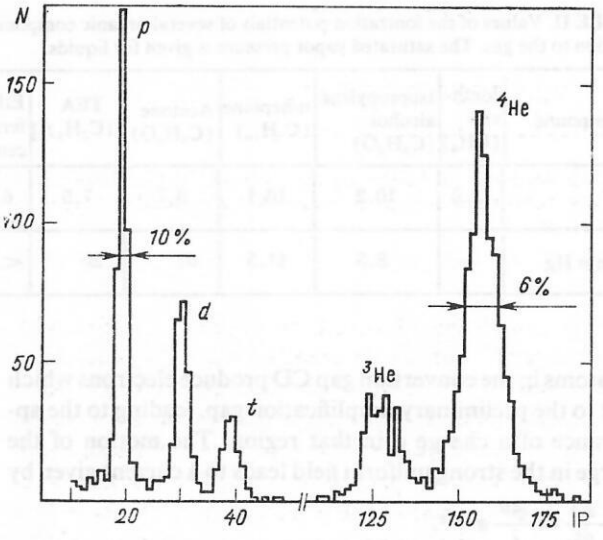

FIG. 24. Event distribution in the identification parameter IP (the mass distribution of hydrogen and helium isotopes) (Ref. 81).

The multistep parallel-plate chamber shown schematically in Fig. 26 has been proposed as a TPD with improved temporal properties and spatial resolution. The electrode 4 is printed on metallized glass laminate and is used to determine the X and Y coordinates, while the other electrodes are wires. The gas is 90% argon and 10% methane. The total gas amplification of the detector is 3×10^5, of which 10^4 is attained in the first gap (2–3) and 30 in the second (3–4). The efficiency of transferring shower electrons to the second gap is 50%. The detected signal is determined by the fast electronic component, and the basal width of the signals is about 8 nsec. The spatial resolution of the detector for soft x-ray radiation is $\sigma = 150\,\mu$m. The two-track resolution is about 1 mm.[85]

4. MEDICAL DIAGNOSTICS

Gamma chambers

The ability of many organs to selectively absorb chemicals enriched by radionuclides has been widely used for functional diagnostics in nuclear medicine. Since particle radi-

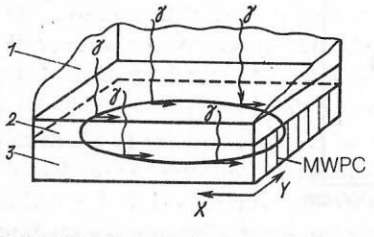

FIG. 25. Schematic depiction of the use of a TPD to detect Vavilov–Čerenkov radiation in a relativistic particle detector (Ref. 71): 1—gas radiator; 2—quartz window; 3—conversion-drift gap.

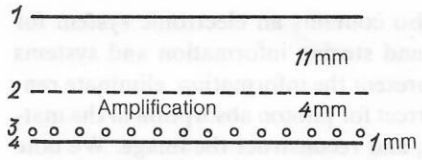

FIG. 26. Multistep parallel-plate chamber (Ref. 85): 1–4 are the detector electrodes. The detected particle interacts with the gas inside the detector in the drift gap.

ation is completely absorbed by organs, nuclides with monoenergetic γ radiation are used for radiopharmaceutical preparations (RPP). When electronic detectors are used to detect radiation harder than the principal type, an effect occurs which is analogous to the appearance of fogginess in photographic film, so that the contrast of the picture is reduced. Currently, one of the principal areas of research in radiopharmaceutical chemistry is the development of new RPP tagged by short- and ultrashort-lived radionuclides.[86] The short half-life and other nuclear physical properties of these RPP make it possible to minimize the radiation dose to the patient, study dynamical processes, and, if necessary, carry out repeated examinations. This requires special complexes consisting of a cyclotron, a radiochemical laboratory, a clinic, and also high-speed detection apparatus.

In functional investigations the internal organs are visualized using classical gamma chambers, in which the radiation is detected by a NaI(T1) crystal of diameter up to 400 mm and thickness of about 10 mm. The scintillation coordinates are determined by a matrix of photomultiplier tubes. The RPP distribution in the organ under study is projected via a collimator onto the entire sensitive area of the detector simultaneously. The spatial resolution, which is defined as the FWHM of the image of a point source at a distance b from the surface of the collimator, is[87] $r_{\text{col}} = d(b + c + a - 2\mu^{-1})/(a - 2\mu^{-1})$, where d is the dimension of the apertures of the collimator, a is the collimator thickness, c is the distance between the closest surface of the collimator and the "effective" plane of the detector, and μ is the linear attenuation coefficient in the material. The geometrical acceptance is $\Omega = [kd^2/(a - 2\mu^{-1})(d + t)]^2$, where t is the thickness of the walls between the apertures of the collimator and k (< 1) is a coefficient depending on the shape of the apertures and their locations. The spatial resolution of the system is determined mainly by the collimator, since $r_c^2 = r_{\text{d}}^2 + r_{\text{col}}^2$, where r_{d} is the intrinsic resolution of the detector and r_{col} is the collimator resolution. The examination time is determined by the efficiency of the system. When the information density is low, statistical fluctuations can distort the image. If the information density in adjacent cells of the detector is N and $N + \Delta N$, the standard error of the counting difference between them is $\sigma_\Delta = \sqrt{2N}$. This is about 10% for a variation of the counting density which can be detected visually in the image.[88] The information density per cell of area $N = 200g^2$ events, where $g = 1, 2, 3$, specifies the number of standard deviations σ_Δ through the relation $\Delta N = g\sigma_\Delta$, that is, 68.3, 95.3, or 99.7%. The examination time is

$$t = \frac{5.4 \cdot 10^{-9}\, g^2 S}{A\Omega\varepsilon},$$

where S is the area of the organ with cumulative activity A (~ 10 mCi), Ω is the geometrical acceptance (determined by the collimator), and ϵ is the detector efficiency.

Traditional gamma chambers use a large number (up to 91) of PM tubes[89] and are not very fast. The typical energy resolution for quanta of energy 140 keV is 15% (Ref. 4) and $r_{\text{d}} = 9$–4.4 mm (Ref. 89); these parameters worsen rapidly with decreasing energy. For example, the energy resolution of crystals of large area for photons of energy in the range from 50 to 100 keV is about 30%–35% (Ref. 90).

Fast gamma chambers based on MWPC[91–94] allow the use of RPP with radiation energy below 100 keV, e.g., ^{197}Hg, ^{133}Xe, ^{178}Ta, ^{201}Tl, and so on. In Fig. 27 we show a detector of sensitive area 27×27 cm^2 filled with a mixture of 90% Xe and 10% CH_4 at a pressure of up to 10 atm. The drawbacks of such detectors are, first of all, the large thickness (about 8 cm), which affects r_{col}, and, secondly, the presence of background signals from fluorescent radiation quanta (point 2 in Fig. 27), which reduces the contrast of the image and lowers the efficiency, since some events are rejected. In Fig. 28 we show the dependence of the detector efficiency on the photon energy at a pressure of about 500 kPa, including and neglecting electronic event rejection. The coordinate information is extracted from the cathodes of the MWPC using DL, and the anode signal is used for amplitude selection. The detector possesses good area uniformity. For example, for 60-keV photons the efficiency is 40% and $r_{\text{d}} = 1.5$ mm (Ref. 92). The energy resolution is about 30%.

When used to detect radiation of energy below 100 keV, a gamma chamber based on an MWPC can be used to obtain more qualitative information than a traditional detection system during a given operating time.[92] This is consistent with the estimates that can be obtained using the expressions given above, taking into account the parameters of the setup and the geometry of the photography. Studies with gamma chambers based on MWPC have shown that they can be used

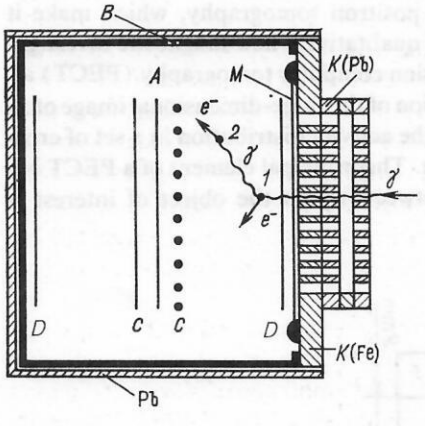

FIG. 27. Schematic depiction of the detector: A—the anode; C—the MWPC cathodes; D—the electrodes of the drift gaps; B—the box; Pb—the lead shield; K(Fe)—a stable flange supporting the entrance window M; K(Pb)—the collimators. Point 1 is where the primary photon undergoes conversion on the Xe atom. The production of a photoelectron on the L shell of the atom by a fluorescent radiation quantum can occur at point 2.

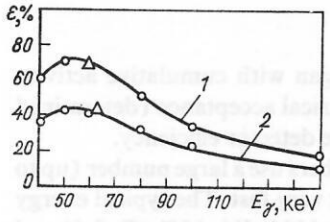

FIG. 28. Dependence of the efficiency of detecting radiation which has passed through the collimator on the photon energy. Curve 1 corresponds to the total number of photon interactions in an 8-cm-thick layer of xenon at a pressure of 500 kPa, and curve 2 is the same after event selection.

to determine the functional state of the heart, the brain, and the kidneys. When the pressure is raised to 1000 kPa, it is possible to use ^{99m}Tc (140 keV), although the examination time increases by a factor of 1.5–2. An electronic detector ensures a speed of response of up to 2.5×10^5 events per second and has stable characteristics when designed properly. Gamma chambers with a large sensitive area can be constructed at relatively low cost.

Work on the design of a gamma chamber capable of operating in a broad range of photon energies has led to the development of the prototype shown in Fig. 29 (Ref. 95). A detector 11 cm in diameter is filled with Xe at a pressure of 10–40 atm. The photons interact with the xenon gas atoms in the gap 1–2 (it is proposed that a layer of liquid Xe be put here). The electrons drift under the influence of the electric field and intersect the wire electrode 2 and then 3. At these instants of time (t_1 and t_2) the PM tube detects scintillation bursts. Since electrode 3 makes an angle of 4° with electrode 2, the difference $t_1 - t_2$ determines the X coordinate. The use of an additional electrode suitably oriented makes it possible to determine a second coordinate of the conversion point.

Emission tomography

The development of the mathematical apparatus for the three-dimensional reconstruction of an object has led to the creation of medical x-ray tomographs and in nuclear medicine has generated interest in single-photon emission tomography (PET) and positron tomography, which make it possible to carry out qualitatively new diagnostic investigations. Positron emission computer tomography (PECT) allows the reconstruction of the three-dimensional image of an object by obtaining the activity distribution in a set of cross sections of the object. The principal element of a PECT is a pair of detectors between which the object of interest is placed. The PECT also contains an electronic system for selecting, recording, and storing information and systems which process and represent the information, eliminate random coincidences, correct for photon absorption in the matter and for scattering, and reconstruct the image. We note that an intrinsic, "electronic" collimation is present when positron RPP are used. The PECT which have been developed are, as a rule, designed for examining the entire body; the possibility of using them for PET when the energies of the emitted photons are below 500 keV is envisioned.

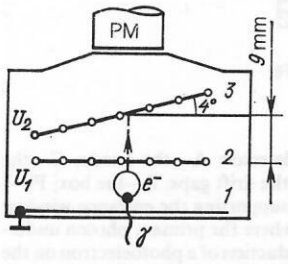

FIG. 29. Schematic depiction of a photon detector filled with pure xenon at a pressure of up to 40 atm.

The annihilation of the emitted positron results in the creation of a pair of 511-keV photons which travel in opposite directions. These photons are detected efficiently using detectors based on a high-density material containing elements of high atomic number. In scintillation PECT (BGO or CsF detectors) the temporal resolution is 15–20 nsec (Ref. 96) or ~5 nsec (Refs. 97 and 98), respectively. Such systems contain hundreds of crystals and are characterized by a small geometrical acceptance. When gaseous coordinate detectors are employed to detect the radiation, either plane convertors of Pb (CP) or convertors with drift channels (CD) of Pb–Bi or Pb-glass are used. The conversion electrons traveling from the walls of the convertor to the gas channels under the influence of the electric field drift into the sensitive region of the MWPC, where they are detected. The sensitivity of the setup can be characterized by the ratio ϵ_2/τ, where ϵ is the detector efficiency and τ is the time resolution. A setup based on an MWPC obviously has a lower sensitivity than a scintillation setup, but it is simpler and has a larger field of view. In Table III we give the parameters of setups based on MWPC used for existing and projected studies under clinical conditions.

A low-pressure light-sensitive coordinate detector combined with a BaF_2 crystal serving as the photon convertor could be the basis for a detector satisfying all the requirements imposed on PECT. Liquid TMAE is used for the photocathode.[99,100]

Digital radiography

Angiography. X-ray studies of blood vessels (angiography) are performed by introducing an x-ray-contrasting material (a preparation of up to 50% iodine) into the artery under study by means of a catheter. It was proposed and then experimentally verified[107,108] that such studies can be carried out using monoenergetic beams of synchrotron radiation (SR), for which it is sufficient to have a concentration of less than 1% of the contrasting material in the blood, which can easily be attained by internal injection. In this procedure the organ is irradiated twice. The first time the beam energy is lower than the K absorption edge of iodine (33 keV), and the second time it is above it. For photons of these energies the absorption coefficient μ in bone and soft tissue varies only insignificantly, while in iodine it varies greatly. The difference between the logarithms of the count in the two measurements is proportional to $\Delta\mu_I x_I$, where x_I is the thickness of the iodine layer. In order to detect an iodine layer $\leqslant 1$ mg/cm^2 thick, it is necessary to ensure that $\Delta N/N \sim 0.01$ (Ref. 109), where N is the count from an ele-

TABLE III. Parameters of setups based on MWPC for positron tomography.

Number of MWPC	MWPC size, cm²	The convertor in each MWPC	Quantum efficiency, %	τ, nsec	Spatial resolution, mm (FWHM)	Reference
2	20×20	CD, Pb–Bi 2×75×0.25 mm³	8,5	20	2,5	[101, 102]
4×4	30×30	CD, Pb–Bi 2×75×0.25 mm³	20	20	2.0	[102]
6	45×45	CD, Pb-glass 2× ×20 mm³	15	200	4.8	[103]
6×2	45×45	CD, Pb-glass 2× ×10 mm³	22,5	100	4,5	[104] *
2×20	30×30	CP, Pb 2×0.125 mm³	6.5	52	5	[105]
2×20	80×40	CP, Pb	14	54	5	[106] *

*Planned systems.

ment of area 0.5×0.5 mm². The required statistics per cell of this area is $(2–8)\times10^4$ events (see the beginning of Sec. 4). To obtain such statistics during the rest time of the heart muscle (0.4 sec), the speed of response must be $(2–8)\times10^5$ events/(mm²·sec).

A parallel beam of monoenergetic SR passes through the object under study and falls on the detector (Fig. 30), which contains 10 wire chambers operating at a rate of up to 4×10^5 events/(mm²·sec). The chambers are designed to have different thicknesses in order to ensure equal charge loading. The sensitive region of the detector has volume $10\times10\times20$ cm³. When the chambers are filled with a mixture of gases consisting mainly of Xe at a pressure of 400 kPa, the efficiency is 95%. The detector is designed for low-dosage angiography setups.[109]

Radiography using monoenergetic γ-ray sources. A monoenergetic x-ray source has been created for systematic studies with various radiography setups.[110] This source contains the usual diagnostic x-ray tube, a target, and a filter composed of various elements, which can be used to obtain monoenergetic beams with energy in the range from 15 to 70 keV. At a distance of 1 m from the filter the area of the photon beam, which has uniform intensity, is 10×10 cm². The integrated intensity of the beam is about 1% of the intensity of the primary polyenergetic beam. It is possible to design a radiography setup with spatial resolution of less than a millimeter using a similar sort of fluorescent monoenergetic source combined with a gaseous coordinate detector possessing a sufficiently high quantum efficiency.[111] The setup is shown schematically in Fig. 31. The x-ray radiation is incident on a target making an angle of 45° with the primary beam. The fluorescent radiation from the target passes through a filter whose K absorption edge lies between the K_α and K_β lines of the target. In Table IV we give combinations of target (of thickness 0.7 mm) and filter materials together with the energy of the monoenergetic radiation.

A monoenergetic γ flux is incident on an MWPC of sensitive volume $128\times128\times6.4$ mm³. Owing to the small thickness of the chamber, the error in the determination of the coordinates for various angles of the photons entering the detector (the "parallax") is no more than 0.4 mm. The intensity of the γ flux over the entire area of the MWPC is 2×10^6 sec^{-1}. The coordinate information is read out from cathode strips of width 2.7 mm by delay lines. The thickness of the entrance window is 0.18 g/cm², and the chamber is filled with a mixture of 80% Xe and 20% CO_2 at a pressure of 200 kPa. The efficiency of detecting 45-keV photons is 10%, the energy resolution is 30%, and the spatial resolution is 0.75 mm. It has been shown that the speed of response of the system can be raised to 10^6 sec^{-1} and that the system can be used for diagnostic purposes.

It is possible to use SR to produce a high-intensity monoenergetic γ beam for low-dosage radiography by using

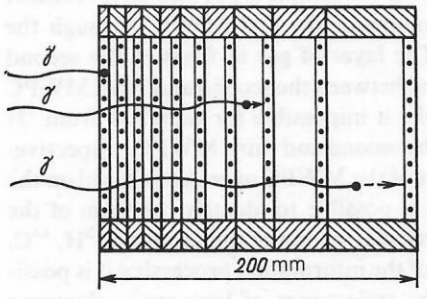

FIG. 30. Angiography detector containing 10 position-sensitive elements consisting of thin MWPC with drift gaps of various sizes. The total number of anode wires is 400.

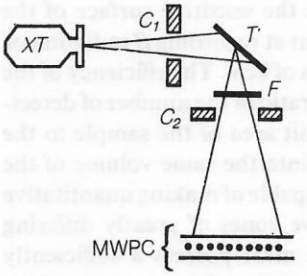

FIG. 31. Schematic depiction of an x-ray setup: XT—x-ray tube; C_1 and C_2—collimators; T—target; F—filter.

TABLE IV. Several combinations of target and filter materials ensuring a monoenergetic photon beam.

Target	Filter	Beam energy, keV
Sm	Nd	40
Gd	Sm	42
Dy	Gd	45

fast gas-filled coordinate detectors of this type with a sufficient large area and relatively high quantum efficiency.

5. ANALYSIS OF RADIOCHROMATOGRAMS

Thin-layer radiochromatography

Chromatography is a method of isolating, analyzing, and chemically studying materials. It has broad applications in biochemistry, molecular biology, pharmacology, medicine, and so on. The method is based on use of the velocity to distinguish components of different mass transported in a flux of liquid along a layer of sorbent. Amounts of matter as small as 1 ng can be distinguished using thin-layer chromatography. Complex protein systems are usually separated into their components by electrophoresis—the directed motion of large protein molecules in an electric field. Biologically active materials are usually labeled by one of the radionuclides ^{3}H, ^{14}C, ^{32}P, ^{35}S, or ^{125}I; double and even triple tagging is possible. In the analysis of radiochromatograms it is first ascertained that the individual components are separated; then, quantitative estimates are made of the percentage radionuclide concentration in the isolated components and the absolute concentration is measured by detection of the β radiation (or γ radiation in the case of ^{125}I).

The traditional methods of analyzing thin-layer samples are characterized by their low sensitivity and large required time (autoradiography) or by the great amount of labor involved (when liquid scintillation counters are used). The nuclear-physics techniques of radiation detection that have been developed recently allow such investigations to be carried out using digital radiography while preserving the material so that more work can be done on it.

The radionuclide is distributed uniformly throughout the thickness of the chromatogram or gel; the effective thickness of the sample is determined by the mean free path of an electron of the maximum energy. For example, for ^{3}H in water, $R_{max} \simeq 0.5$ mag/cm^2 (i.e., 5 μm) and for ^{14}C, $R_{max} \simeq 27.6$ mg/cm^2. The sample under study obviously must be in direct contact with the sensitive surface of the detector, which is highly efficient at recording β radiation of energy from several to hundreds of keV. The efficiency of the analysis is characterized by the ratio of the number of detected events per second from a unit area of the sample to the amount of activity introduced into the same volume of the sample. The detector must be capable of making quantitative measurements when radioactive zones of greatly differing activity are present, that is, it must possess a sufficiently large dynamical range. The sensitivity of the method, which is determined by the background level (1 cm$^{-2}\cdot$min^{-1}), is limited by the intrinsic noise of the detector, which must be stable in time. The spatial resolution characterizes the ability to separately detect radioactive zones which are close together. It should be noted that as long as the detected peaks are Gaussian, by analyzing them it is possible to distinguish them even when they have different heights and overlap significantly.

There have been some attempts to use spark chambers for two-coordinate analysis of chromatographs; however, these have not received wide application because of technical difficulties and the impossibility of making quantitative measurements. One-coordinate counters are widely used for scanning planar samples. The possibility of using MWPC to analyze radiochromatograms was pointed out in Ref. 112, which led to the creation of specialized setups at a number of scientific centers.[113–116]

One-coordinate detectors

The typical one-coordinate detector of a scanning setup for analyzing planar samples consists of a proportional counter with an anode wire fixed in the center of the detector. The sensitive area of the detector is 250×15 mm^2. The coordinate information is read out from two ends of the DL forming part of the cathode. The detector has two operating modes: one with the entrance window covered by aluminized mylar (Al-mylar) of thickness 12 μm and when detecting tritium radiation ($E < 18$ keV), another with the window open, in which case the Al-mylar is replaced by a wire electrode. The detector operates at a gas (Ar plus 10% CH_4) flow rate of about 300 cm^3/min. The spatial resolution, which is defined as the minimum distance between adjacent, fully distinguishable zones of equal activity, is 0.8 mm for ^{3}H and 3 to 4 mm for ^{14}C ($E < 155$ keV). The sensitivity is about 20 pCi/mm for ^{3}H and 2 pCi/mm for ^{14}C (Ref. 117).

MWPC with cathode readout for digital autoradiography of planar radiochromatograms

Setups based on MWPC with cathode readout of the coordinate information using DL have been developed at the JINR High Energy Laboratory for the automatic express analysis of thin-layer radiochromatograms.[113,114] The detector consists of three MWPC with the drift gaps located inside a hermetically sealed box which has been flushed with a gaseous mixture.[118] The flat sample of area up to 200×200 mm^2 which is to be analyzed is introduced into the detector. The irradiated surface of the sample is put into direct contact with the sensitive volume of the first MWPC through the narrow drift gaps. The layer of gas in front of the second MWPC and the Al foil between the second and third MWPC act as filters and make it impossible for radiation from ^{3}H and ^{14}C to travel to the second and third MWPC, respectively. Statistical analysis of the MWPC operations based on the anode signals makes it possible to identify the form of the radionuclide in a particular region of the sample as ^{3}H, ^{14}C, or ^{32}P. In the course of the information processing it is possible to reconstruct the trajectories of long-range electrons and to determine the point at which they were emitted from the sample, which, in spite of the large amount of Coulomb

TABLE V. Basic parameters of a radiochromatograph based on an MWPC for several radionuclides.

Nuclide	Spatial resolution, mm	Sensitivity, pCi/mm^2
^{3}H	1—1.5	10
^{11}C	6	0.5
^{32}P	10 (4)	0.1 (0,3)

scattering, allows the spatial resolution to be increased for ^{32}P ($E_{max} = 1.7$ MeV). The basic parameters of the setup are given in Table V. Inside the parentheses are the values obtained by reconstruction of the emission point.

It should be noted that the need for introducing the sample into the gas-filled region of the detector complicates the construction and makes it necessary to have an experienced operator. The use of such a setup for biochemical research gives an increase in the speed by more than a factor of 100. The analysis of a radiochromatogram usually takes no longer than 30 min. A complete analysis of a peptide chart has been done in, for example, 1.5–2 hours, with the peptide sample preserved for further study. A comparable analysis using liquid counters requires slicing the chromatogram into 1500 to 2000 samples, finding their counts, and then reconstructing the chart. The biological material cannot be reused after this procedure. It is possible to use an MWPC to perform a quick analysis of an iodized mixture of proteins with high spatial resolution (about 1 mm).[119]

An MWPC has been used to study the DNA replication mechanism by digital autoradiography of living cells tagged by ^{3}H or ^{14}C (Ref. 120). When working with tritium the samples are put inside the detector because of the small electron mean free path. When the gas in the detector is at standard pressure the spatial resolution is 1.5 mm (FWHM), and at a pressure of 202 kPa it is 0.8 mm.

When working with ^{14}C and ^{32}P the chromatograms can be placed inside the gas-filled region of the detector on a thin-film entrance window. The spatial resolution is determined by the quantity $l \tan \Theta$, where l is the effective thickness of the detector and Θ is the angle at which the radiation enters the detector. We note that when, for example, 100-keV electrons pass through polyethylene of thickness 1 mm the average angle of their Coulomb scattering is 70°. The minimum thickness of the MWPC is 2 mm (Ref. 121). This chamber operates in the SQS mode and has a gas amplification of 10^7. The possibility of using such devices to detect soft β radiation is determined by the minimum possible thickness of the entrance window, which also serves as the cathode of the MWPC.

Radiochromatographs based on MSSC

The use of an MSSC as a detector with focusing properties to record the β radiation from ^{14}C, ^{32}P, or ^{35}S leads to a higher spatial resolution and improves the operational features of the radiochromatograph (Fig. 32).[122] An MSSC with sensitive area 160×160 mm^2 records the coordinates of the points at which particles enter the plane of the entrance window with a spatial resolution of about 1 mm for all the nuclides. The detector is flushed with a mixture of Ar gas with 1.5% n-heptane, and a constant value of the partial pressure is ensured by passing all the Ar gas through n-heptane at 0 °C. The nonuniformity in the area of the detector is less than 5%, and the setup is characterized by a high degree of stability and reproducibility of the measurements. The analysis time is no greater than 30 min, and the sensitivity is 1 pCi/mm^2 for ^{32}P and ~3 pCi/mm^2 for ^{14}C and ^{35}S. The characteristic radiation of ^{125}I (4 keV) can be detected with an efficiency of about 3%. Here the spatial resolution is about 1 mm, and the sensitivity is 6 pCi/mm^2. The regulators of cell metabolism and processes related to biosynthesis are studied using this setup. A cycle of studies on the identification of ribosomal proteins has been carried out. Radioimmunological analysis (RIA) has many applications in medicine, biology, biochemistry, pharmacology, and agriculture. The use of the most promising RIA technique, the solid-phase technique, is limited by the lack of instrumentation for the miscounting of the standard 96- and 60-hole plane tables. The measurements are obtained by successively finding the miscounting for each hole using a gamma counter. In this setup it is possible to obtain miscounting of the standard plane tables adjusted to the detector using collimators whose

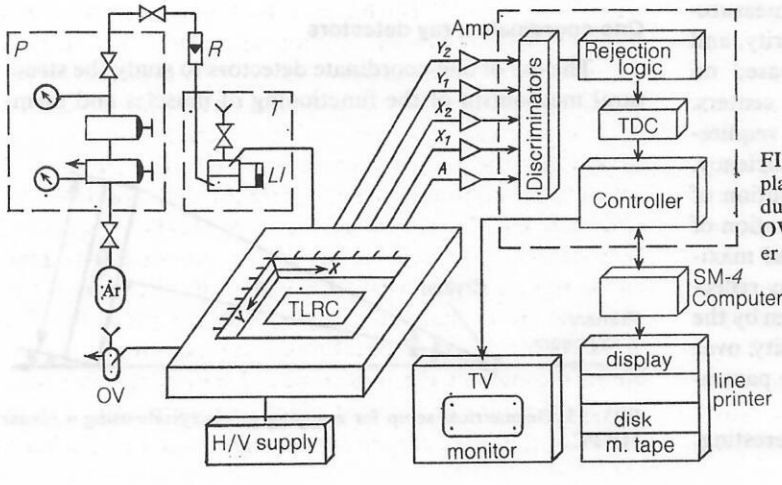

FIG. 32. Block diagram of a setup for the express analysis of planar radiochromatograms and electrophoregrams: P—reductor; R—rotameter; T—thermostat; LI—level indicator; OV—oil stop-valve; Amp—amplifiers. TLRC—the thin-layer radiochromatogram under study.

geometrical parameters correspond to those of the plane tables. The collimators limit the photon radiation and the characteristic radiation of energy of about 30 keV without appreciably affecting the efficiency of detecting 4-keV photons. The low intrinsic noise level of MSSC (~ 3 $\text{min}^{-1} \cdot \text{cm}^2$) ensures a sensitivity of 500 and 700 min^{-1} per hole for the 60- and 96-hole plane tables, respectively. The activity during the analysis is usually about 10^4 min^{-1} per hole. Such setups allow the broad application of RIA for the quantitative and qualitative analysis of antibodies, hormones, nucleic acids, pharmacological preparations, pesticides, and so on.[123]

6. THE USE OF MWPC FOR STRUCTURAL ANALYSIS

Requirements of x-ray detectors

X-ray structural analysis (XSA) is based on measurement of the spatial distribution and intensity of x-ray of wavelength λ from 0.25 to 0.06 nm (5–20 keV) scattered by the sample under study. The intensive development of XSA is a consequence of the existence of x-ray tubes, which make it possible to obtain intense beams, the possibility of using high-intensity synchrotron radiation, and the existence of efficient radiation detectors. When studying the structure of complex crystals it is necessary to measure tens and hundreds of thousands of reflections of varying intensity, so the measurement time must be large in order to ensure a statistical accuracy of at least a few percent. Consequently, the time needed for the experiment may not be compatible with the "lifetime" of the crystal if its resistance to radiation is low. A study of the crystal of the vitamin B_{12} containing 95 atoms, for example, requires a photograph resolution $d = 0.1$ nm and the recording of 3200 independent reflections. The tobacco virus crystal (TMV) containing 6000 000 atoms requires a resolution $d = 0.28$ nm and 2×10^6 independent reflections.[124] Such objects obviously must be studied using large-area detectors and a high degree of automation. The traditional detector, photographic film, has a high quantum efficiency (65% for CuK_α radiation), but its intrinsic background is about 10^6 photons/mm^2, which limits the lower level of measurable intensities, the dynamical range of the counting, and the measuring accuracy. It also makes it difficult to attain a high level of automation. Fast scanning television systems have recently been designed for XSA, but they are not good enough for making quantitative measurements because of the high noise level, the nonlinearity, and the narrow dynamical range. Diffractometers based on MWPC have been constructed at many scientific centers. These come closest to satisfying the following basic requirements of diffraction experiments: high quantum efficiency, good spatial resolution ensuring the angular resolution of closely spaced diffraction images, energy discrimination of the detected radiation, minimal time resolution and maximum speed of response, the ability to measure many reflections simultaneously, small detector thickness as seen by the beam, a sufficiently large area, maximum reliability over long-term operation, and temporal stability of the parameters.

The MWPC with a spherical drift gap[125] is interesting, but planar MWPC are of most interest for XSA because of their superior operating characteristics.

X-ray diffractometers with planar MWPC

A shortened photography time with a simultaneous decrease of the amount of radiation exposure of the sample are determined by the quantum efficiency, the number of resolving elements in the detector, and the response time. To optimize the geometrical parameters of the photography, the MWPC are arranged such that the normal to the detector plane makes a Bragg angle $\Theta = \arcsin \lambda / 2d$ with the direction of the primary beam (Fig. 33), where d characterizes the resolution of the photograph and can be written as $d = \lambda (2 \sin \arctan L/2R)^{-1}$. The linear dimension of the reflections Δ_l is determined by the spatial resolution Δ of the system for normally incident beams, by reflection broadening due to parallax, and by the dispersion of the diffracted beams $d\Theta$: $\Delta_l = \Delta + g \tan \Theta + Rd\Theta \cos^{-2} \Theta$, where g is the effective thickness of the detector determined by taking into account the exponential nature of the absorption of the radiation. The angular resolution of the system is $\delta = \Delta_l R^{-1} \cos^2 \Theta$. The maximum lattice spacing of the crystal $a_{\max}$ which can be studied in the diffractometer is estimated from the expression $\delta = \lambda / a_{\max}$. We note that the number of simultaneous reflections increases with increasing $a_{\max}$.

The first MWPC-based XSA system in the USSR was built at the Institute of Nuclear Physics of the Siberian Division of the USSR Academy of Sciences and was used to study biopolymers by means of synchrotron radiation.[126] Later setups developed at that laboratory and at the Joint Institute for Nuclear Research are used for the XSA of protein monocrystals. In Table VI we give the basic parameters of the most efficient diffractometers based on planar MWPC. In all cases the chamber is flushed with a mixture of gases based on xenon. The use of, for example, the KARD-3 diffractometer has made it possible to decrease the experiment running time by a factor of 50 with a corresponding decrease of the radiation dose compared to the inclined single-channel diffractometer used previously. Mappings of 40 proteins with molecular masses of up to 200 000 and including some which are unstable to radiation have been made at the KARD-3 installation.

One-coordinate x-ray detectors

The use of one-coordinate detectors to study the structural mechanism of the functioning of muscles and mem-

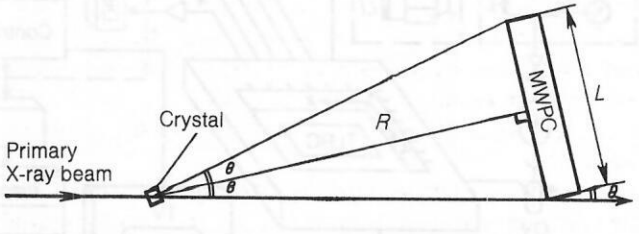

FIG. 33. Geometrical setup for mapping monocrystals using a planar MWPC.

TABLE VI. Operational diffractometers based on MWPC.

Fundamental parameters of the system	KARD-3 (Refs. 127, 128)	KARD-4 (Ref. 129)	MAD (Ref. 130)	ARGUS (Ref. 131)
Effective volume of detector, mm^3	320×320×10	420×420×10	300×270×9	256×256×9
Spatial resolution, mm				
X	1.4	1.8	1.17	2
Y	1.6	2.0	2.13	2
Number of channels	256×200	256×210	256×128	128×128
Efficiency for CuK_α, %	70	70	50	60
Nonuniformity of efficiency, %	2	2	2	—
Nonuniformity of channel width, %				
X	2	2	5	~5
Y	4	4	2.5	~5
Number of measured orders of reflection	9—12.5	10—13	9.5	6—15
a_{max}, nm	0.16—0.27	0.13—0.19	0.22	0.18—0.5
d, nm	56—46	77—66	43	33—30
Maximum counting rate for losses <25%, sec^{-1}	$2.5 \cdot 10^5$	$2.5 \cdot 10^5$	$6 \cdot 10^4$	$3 \cdot 10^5$
Readout method	Delay lines (DL)	DL	DL	Digital

branes[132] and to investigate the structure of various materials at high pressures and temperatures, etc., by means of small-angle diffractive scattering began with the development of a counter with a resistive anode wire, with the coordinate information determined from the rise time of the leading edge of the output pulse.[134]

Now most small-angle diffractometers make use of one-coordinate detectors consisting of MWPC with one-coordinate readout via a DL which is part of the cathode. The anode is of the multiwire type and the entrance window is vacuum-tight beryllium of thickness up to 1 mm. It is filled with a gas consisting of 90% Xe and 10% CH_4 at a pressure of up to 500 kPa. The quantum efficiency is no worse than 50%. The spatial resolution is 0.3 mm for MoK_α and 0.1 mm (FWHM) for CuK_α and is restricted by the mean free paths of the shower electrons. The energy resolution is 30%–40%. It should be noted that for an MWPC with Xe it gets harder to obtain good energy resolution and a large signal-to-noise ratio as the pressure is increased. When used for fast, multiframe x-ray photography, this sort of one-coordinate detector ensures a speed of response of up to 2.5×10^5 events per second and can be used successfully in an SR beam.[133]

The use of such detectors in wide-angle diffractometers for studying polycrystals is limited by the smaller spatial resolution for beams entering a planar detector at large angles. To correct this, a detector has been designed with a single anode wire of diameter 38 μm and length 20 cm bent into an arc of radius 29 cm (Ref. 135). When this wire, placed in a magnetic field of strength 800 G, is in its stable position, a current of 15 mA flows through it. The information is read out from a DL, and the detector thickness as seen by the beam is 12.5 mm. It is filled with 90% Xe and 10% CH_4 gas at a pressure of 300 kPa. The spatial resolution is 0.3 mm (FWHM), and the angular aperture is 40°.

In Fig. 34 we show a detector with radius of curvature 20 cm and anode in the form of a sharp edge. The detector thickness is 8 mm. The rear cathode consists of 94 strips of width 2 mm. The information is read out from the strips

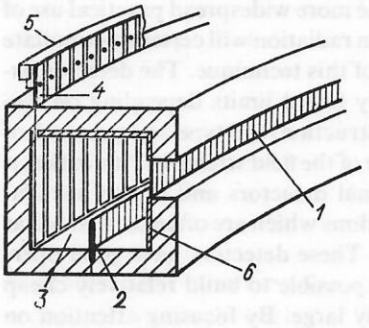

FIG. 34. A one-coordinate detector of radius of curvature 20 cm: 1—entrance window; 2—anode; 3—sensitive gas-filled region of the detector; 4—cathode strips; 5—delay lines; 6—elements of the detector cathode.

using DL. A steel plate of thickness 40 μm serves as the anode. The detector operates in the SQS mode at a pressure of 200 kPa, and the signal-to-noise ratio is over 100. The entrance window of width 10 mm is made of Al-mylar of thickness 25 μm. The spatial resolution is 0.18 mm (FWHM) for CuK_α, and the angular aperture is 60° (Ref. 136).

Neutron diffractometry

Some investigations, such as the study of magnetic materials, the determination of the positions of light atoms in a substance, and the determination of the difference of atoms with nearly equal atomic numbers, can be carried out only by neutron-diffractometry techniques. The method of small-angle scattering is widely used at neutron sources to solve structural problems in solid-state physics, biology, polymer physics, and materials science.[137] A setup with an annular multiwire ^{3}He detector of slow neutrons with 70% detection efficiency ($\lambda = 0.18$ nm) has been constructed at the Joint Institute for Nuclear Research to carry out such investigations using the IBR-2 reactor.[138] The time-of-flight diffractometer designed for structural studies of protein monocrystals at the IBR-2 is based on a two-coordinate MWPC with digital information readout from the cathode wires.[137] Neutrons are detected via the reaction $^3He(n,p)^3H$ with efficiency equal to 63% and 86% for neutrons of wavelength 0.2 and 0.4 nm, respectively. The pressure of the gaseous mixture in the detector is 600 kPa, the partial pressures being 250 kPa for He, 350 kPa for Ar, and 45 mm Hg for CH_4. The presence of Ar decreases the mean free path of the nuclear reaction products, which limit the spatial resolution to 0.31 mm.

CONCLUSION

Wire gaseous coordinate detectors of charged radiation, neutrons, and gamma, x-ray, and ultraviolet radiation currently have broad applications not only in experimental nuclear physics, but also in quite different areas of research. These detectors are widely used in astrophysics. The possibilities of using them effectively in medicine for diagnostic purposes are being investigated. They play an important role in a number of areas of biomedical research such as the detection of soft β and γ radiation in analyzing planar radiochromatograms or phoregrams, immunology, and x-ray structural analysis. The use in medical diagnostics of short-lived radionuclides and the more widespread practical use of high-intensity synchrotron radiation will certainly stimulate the further development of this technique. The detector parameters vary within very broad limits depending on features of the detector construction, the type and pressure of the gas used, and the value of the field strength. This makes it possible to develop original detectors and create installations for automatic operations which are often carried out at a qualitatively new level. These detectors have good operational features, and it is possible to build relatively cheap ones which are sufficiently large. By focusing attention on certain fundamental parameters of these detection systems it is possible to solve in the most rational way many important problems arising both in experimental nuclear physics and in other areas of science and technology to which nuclear-physics techniques are applicable.

In conclusion, the author would like to thank Academician A. M. Baldin for his interest in and support of this study, and Yu. V. Zanevskiĭ, I. F. Kolpakov, and M. D. Shafranov for useful discussions.

[a] 1 mm Hg is 1.33×10^2 Pa.

[1]DELPHI, Technical Proposal, CERN/LEPC/83-3, 1983.
[2]G. Charpak, Usp. Fiz. Nauk **108**, 339 (1972). (Russ. transl.)
[3]F. Sauli, CERN 77-09, 1977.
[4]Yu. V. Zanevskiĭ and V. D. Peshekhonov, Prib. Tekh. Eksp. No. 2, 7 (1978) [Instrum. Exp. Tech.].
[5]Yu. V. Zanevskiĭ, Provolochnye detektory élementarnykh chastits (Wire Detectors of Elementary Particles), Atomizdat, Moscow, 1978.
[6]G. Charpak, Nucl. Instrum. Methods **156**, 1 (1978).
[7]D. F. Anderson, NAL Fermilab-84/116, 1984.
[8]L. S. Gorn and B. I. Khazanov, Pozitsionno-chuvstvitel'nye detektory (Position-Sensitive Detectors), Energoizdat, Moscow, 1982.
[9]A. s. 241553, Ustroĭstvo dlya opredeleniya koordinat mesta proleta zaryazhennoĭ chastitsy (A Setup for Determining the Coordinates of a Charged Particle Trajectory), V. G. Zinov, Otkrytiya, Izobreteniya, No. 14, 1969.
[10]E. J. Kobetich and R. Katz, Phys. Rev. **170**, 391 (1968).
[11]Studies in Penetration of Charged Particles in Matter, Publication No. 1133, National Academy of Sciences, Washington, Report 39, 1964.
[12]A. M. Shapiro, E. D. Aliero, Jr., F. Barreiro *et al.*, Rev. Sci. Instrum. **53**, 393 (1982) (Russ. transl.)
[13]G. I. Merzon, B. Sitar, and Yu. A. Budagov, Fiz. Elem. Chastits At. Yadra **14**, 648 (1983) [Sov. J. Part. Nucl. **14**, 270 (1983)].
[14]J. H. Cobb, W. W. M. Allison, and J. N. Bunch, Nucl. Instrum. Methods **133**, 315 (1976).
[15]V. A. Davidenko, B. A. Dolgoshein, V. K. Semenov, and S. V. Somov, Nucl. Instrum. Methods **67**, 325 (1969).
[16]Heikki Sipilä, Nucl. Instrum. Methods **133**, 251 (1976).
[17]M.-L. Järvinen and Heikki Sipilä, Nucl. Instrum. Methods **193**, 53 (1982).
[18]W. Farr, J. Heintze, K. H. Hellenbrand, and A. H. Walenta, Nucl. Instrum. Methods **154**, 175 (1978).
[19]F. Sauli, CERN-EP/82-130, 1982.
[20]A. H. Wapstra, G. J. Nijgh, and R. Van Lieshout, Nuclear Spectroscopy Tables, North-Holland, Amsterdam, 1959.
[21]K. Siegbahn, Alpha-, Beta, and Gamma-Ray Spectroscopy, North-Holland, Amsterdam, 1965 (Russ. transl., Atomizdat, Moscow, 1969, Vol. 4, pp. 207–272).
[22]K. Valentine, S. Kaplan, L. Kaufman, *et al.*, IEEE Trans. Nucl. Sci. NS-19, No. 1, 374 (1972).
[23]Yu. V. Zanevskiĭ, V. D. Peshekhonov, and L. P. Smykov, R13-84-563, JINR, Dubna, 1984.
[24]G. Melchart, G. Charpak, F. Sauli, *et al.*, Nucl. Instrum. Methods **186**, 613 (1981).
[25]L. Mouchka, V. D. Peshekhonov, B. Sitar, and L. Sitarova, in: Proceedings of the Third Meeting on the Use of New Nuclear Physics Techniques to Solve Scientific, Technical, and Agricultural Problems, JINR, Dubna, 1979, p. 331 (in Russian).
[26]J. M. Meek and J. D. Craggs, *Electrical Breakdown of Gases* (Wiley, New York, 1978) (Russ. transl., Izd. inostr. lit., Moscow, 1960).
[27]J. J. Lowke and J. H. Parker, Jr., Phys. Rev. **181**, 302 (1969).
[28]R. A. Astabatyan, Yu. V. Zanevskiĭ, and V. D. Peshekhonov, R13-8383, JINR, Dubna, 1974.
[29]S. C. Brown, *Basic Data of Plasma Physics* (MIT Press, Cambridge, Massachusetts, 1959) (Russian translation, Gosatomizdat, Moscow, 1961).
[30]A. Peisert and F. Sauli, CERN 84-08, 1984.
[31]G. Charpak, A. Policarpo, and F. Sauli, IEEE Trans. Nucl. Sci. NS-27, No. 1, 212 (1980).
[32]V. M. Golovatyuk, V. D. Peshekhonov, and Yu. V. Zanevsky, Nucl. Instrum. Methods **140**, 259 (1977).
[33]G. D. Alekseev, V. V. Kruglov, and D. M. Khazins, Fiz. Elem. Chastits

At. Yadra **13**, 703 (1982) [Sov. J. Part. Nucl. **13**, 293 (1982)].
[34]V. M. Golovatyuk, Z. Guzik, R. B. Kadyrov, *et al.*, D1-84-405, JINR, Dubna, 1984.
[35]N. A. Kalinina and D. M. Khazins, Prib. Tekh. Eksp. No. 3, 43 (1984) [Instrum. Exp. Tech.].
[36]J. Fischer, H. Okuno, and A. H. Walenta, Nucl. Instrum. Methods **151**, 451 (1978).
[37]G. Charpak, D. Rahm, and H. Steiner, Nucl. Instrum. Methods **80**, 13 (1970).
[38]T. J. Harris and E. Mathieson, Nucl. Instrum. Methods **154**, 183 (1978).
[39]Yu. V. Zanevskiĭ, B. K. Kuryatnikov, V. D. Peshekhonov, *et al.*, in: Proportsional'nye kamery (Proportional Chambers), JINR, Dubna, 1973, p. 37.
[40]B. Makowski and B. Sadoulet, Nucl. Instrum. Methods **111**, 561 (1973).
[41]V. M. Golovatyuk, Yu. V. Zanevskiĭ, and V. D. Peshekhonov, Prib. Tekh. Eksp. No. 6, 30 (1978) [Instrum. Exp. Tech.].
[42]T. Trippe, CERN NP 69-18, 1969.
[43]S. P. Chernenko, N. A. Filatova, A. B. Ivanov, *et al.*, Nucl. Instrum. Methods **114**, 597 (1974).
[44]V. D. Peshekhonov and Yu. V. Zanevsky, Nucl. Instrum. Methods **100**, 505 (1972).
[45]V. Yu. Glebov and A. N. Zelenskiĭ, in Proportsional'nye kamery (Proportional Chambers), JINR, Dubna, 1973, p. 85.
[46]V. R. Groshev and A. P. Onuchin, in Proportsional'nye i dreĭfovye kamery (Proportional and Drift Chambers), JINR, Dubna, 1975, p. 120.
[47]V. G. Ableev, V. A. Aref'ev, S. G. Basiladze, *et al.*, 13-8829, JINR, Dubna, 1975.
[48]P. Coteus, J. Cumalat, *et al.*, Nucl. Instrum. Methods A **222**, 474 (1984).
[49]Yu. S. Anisimov, S. P. Chernenko, A. B. Ivanov, *et al.*, Nucl. Instrum. Methods **176**, 67 (1980).
[50]F. Piuz, R. Roosen, and J. Timmermans, Nucl. Instrum. Methods **196**, 451 (1982).
[51]J. L. Lacy and R. S. Lindsey, Nucl. Instrum. Methods **119**, 483 (1974).
[52]A. E. Bondar', A. P. Onuchin, V. S. Papin, and V. I. Tel'nov, Preprint 82-17, Institute of Nuclear Physics, Siberian Division, USSR Academy of Sciences, Novosibirsk, 1982.
[53]R. Allemand and G. Thomas, Nucl. Instrum. Methods **137**, 141 (1976).
[54]C. Martin, P. Jelinsky, M. Lampton, *et al.*, Rev. Sci. Instrum. **52**, 1067 (1981) (Russ. transl.).
[55]D. F. Anderson, H. K. Arvela, A. Breskin, and G. Charpak, Nucl. Instrum. Methods A **224**, 315 (1984).
[56]M. Starič, D. Zavrtanik, and G. Kernel, Nucl. Instrum. Methods **216**, 67 (1983).
[57]W. J. Price, *Nuclear Radiation Detection* (McGraw-Hill, New York, 1958) (Russ. transl., Izd. inostr. lit., Moscow, 1960).
[58]F. Binon, V. V. Bobyr, P. Duteil, *et al.*, Nucl. Instrum. Methods **94**, 27 (1971).
[59]V. M. Golovatyuk, A. B. Ivanov, V. A. Nikitin, *et al.*, Nucl. Instrum. Methods **145**, 437 (1977).
[60]A. Breshkin, Nucl. Instrum. Methods **196**, 11 (1982).
[61]J. Van Der Plicht and A. Gavron, Nucl. Instrum. Methods **211**, 403 (1983).
[62]D. A. Abduchukurov, Yu. V. Zanevskiĭ, S. A. Movchan, *et al.*, Prib. Tekh. Eksp. No. 6, 37 (1983) [Instrum. Exp. Tech.].
[63]D. F. Anderson, G. Charpak, W. Kusmierz, *et al.*, Nucl. Instrum. Methods A **228**, 33 (1984).
[64]N. A. Filatova, A. Forycki, V. M. Golovatyuk, *et al.*, Nucl. Instrum. Methods **215**, 135 (1983).
[65]Yu. V. Zanevskiĭ, L. Mouchka, T. Petyshie, *et al.*, Jad. Energ. **29**, 148 (1983).
[66]A. Breskin, G. Charpak, B. Gabioud, *et al.*, Nucl. Instrum. Methods **119**, 9 (1974).
[67]J. Allison, C. K. Bowdery, and P. G. Rowe, Univ. of Manchester M81/33, 1981.
[68]A. Franz and C. Grupen, Nucl. Instrum. Methods **200**, 331 (1982).
[69]Yu. A. Budagov, A. P. Nagaĭtsev, A. A. Omel'yanenko, *et al.*, 13-84-394, JINR, Dubna, 1984.
[70]Cr. Becker, W. Weihs, and G. Zech, Nucl. Instrum. Methods **200**, 335 (1982).
[71]D. F. Anderson, IEEE Trans. Nucl. Sci. NS-28, 842 (1981).
[72]G. F. Karabadzhak, V. D. Peskov, and E. R. Podolyak, Nucl. Instrum. Methods **217**, 56 (1983).
[73]D. A. Abdushukurov, Yu. V. Zanevskiĭ, S. A. Movchan, *et al.*, 13-82-216, JINR, Dubna, 1982.
[74]J. R. Hubbard, G. Coutrakon, M. Cribier, *et al.*, Nucl. Instrum. Methods **176**, 233 (1980).
[75]R. Bouclier, G. Charpak, A. Cattai, *et al.*, Nucl. Instrum. Methods **205**, 403 (1983).
[76]P. Mangeot, G. Coutrakon, J. R. Hubbard, *et al.*, Nucl. Instrum. Methods **216**, 79 (1983).
[77]A. Breskin, G. Charpak, and S. Majewski, Nucl. Instrum. Methods A **220**, 349 (1984).
[78]Yu. V. Zanevskiĭ, V. D. Peshekhonov, and L. P. Smykov, R13-84-563, JINR, Dubna, 1984.
[79]A. Breskin, R. Chechik, I. Levin, *et al.*, Nucl. Instrum. Methods **217**, 107 (1983).
[80]A. Breskin and R. Chechik, Nucl. Instrum. Methods A **227**, 24 (1984).
[81]V. A. Budilov, Yu. V. Zanevskiĭ, Yu. Zlomanchuk, *et al.*, Prib. Tekh. Eksp. No. 2, 48 (1985) [Instrum. Exp. Tech.].
[82]W. W. M. Allison *et al.*, Nucl. Instrum. Methods **119**, 499 (1974).
[83]M. Davenport *et al.*, IEEE Trans. Nucl. Sci. **NS-30**, 35 (1983).
[84]L. O. Eek, T. Ekelöf, K. Fransson, *et al.*, IEEE Trans. Nucl. Sci. **NS-31**, 949 (1984).
[85]A. Peisert, G. Charpak, F. Sauli, and G. Viezzoli, IEEE Trans. Nucl. Sci. **NS-31**, 125 (1984).
[86]V. T. Kharlamov, Atomic Energy **55**, 132 (1983).
[87]L. Eldon and A. Keller, J. Nucl. Med. **9**, 233 (1968).
[88]R. P. Parker, P. Smith, and D. Taylor, *Basic Science of Nuclear Medicine*, 2nd Ed. (Churchill, 1984) (Russ. transl., Energoizdat, Moscow, 1981).
[89]J. A. Patton, F. D. Rollo, and A. B. Brill, IEEE Trans. Nucl. Sci. **NS-27**, 1066 (1980).
[90]E. Costa, G. Auriemma, L. Boccaccini, *et al.*, Nucl. Instrum. Methods **156**, 57 (1978).
[91]Yu. V. Zanevskiĭ, K. D. Kalantarov, E. A. Matyushevskiĭ, *et al.*, R13-81-298, JINR, Dubna, 1981.
[92]Yu. S. Anisimov, S. P. Chernenko, G. A. Cheremukhina, *et al.*, Nucl. Instrum. Methods A **235**, 582 (1985).
[93]R. E. Zimmerman, B. L. Holman, F. H. Fahey, *et al.*, IEEE Trans. Nucl. Sci. **NS-28**, 55 (1981).
[94]J. L. Lasy, A. D. Le Blano, J. W. Babich, *et al.*, J. Nucl. Med. **25**, 1003 (1984).
[95]B. U. Rodionov and V. Yu. Chepel', Ustroĭstvo dlya registratsii koordinat chastits v dreĭfovoĭ kamere (A Setup to Record Particle Coordinates in a Drift Chamber), Otkrytiya, Izobreteniya, No. 26, 1983.
[96]K. Takami, K. Ueda, K. Okajima, *et al.*, IEEE Trans. Nucl. Sci. **NS-30**, 734 (1983).
[97]D. C. Ficke, D. E. Beecher, G. R. Hoffman, *et al.*, IEEE Trans. Nucl. Sci. **NS-29**, 474 (1982).
[98]N. A. Mullani, Wai-Noi Wong, R. Hartz, *et al.*, IEEE Trans. Nucl. Sci. **NS-30**, 739 (1983).
[99]D. F. Anderson, Phys. Lett. **118B**, 230 (1982).
[100]D. F. Anderson, R. Bouclier, G. Charpak, and S. Majewski, Nucl. Instrum. Methods **217**, 217 (1983).
[101]A. Jeavons, K. Kull, B. Lindberg, *et al.*, Nucl. Instrum. Methods **176**, 89 (1980).
[102]A. Jeavons, C. Parkman, A. Donath, *et al.*, IEEE Trans. Nucl. Sci. **NS-30**, 640 (1983).
[103]A. Del Guerra, V. Perez-Mendez, G. Schwartz, *et al.*, IEEE Trans. Nucl. Sci. **NS-30**, 646 (1983).
[104]R. Bellazzini, A. Del Guerra, M. M. Massai, *et al.*, IEEE Trans. Nucl. Sci. **NS-31**, 645 (1984).
[105]J. E. Bateman, J. F. Connolly, R. Stephenson, *et al.*, Nucl. Instrum. Methods **217**, 77 (1983).
[106]J. E. Bateman, J. F. Connolly, R. Stephenson, *et al.*, Nucl. Instrum. Methods A **225**, 209 (1984).
[107]H. D. Zeman, E. B. Hughes, L. E. Campbell, *et al.*, IEEE Trans. Nucl. Sci. **NS-29**, 442 (1982).
[108]V. B. Baryshev, in Proceedings of the Fourth Meeting on the Use of New Nuclear Physics Techniques to Solve Scientific, Technical, and Agricultural Problems, JINR, Dubna, 1982, p. 50 (in Russian).
[109]A. N. Walenta, Nucl. Instrum. Methods **217**, 65 (1983).
[110]K. Doi, C. J. Vyborny, and G. Holje, Radiology **142**, 233 (1982).
[111]R. Bellazzini, A. Brez, A. Del Guerra, *et al.*, Nucl. Instrum. Methods A **228**, 193 (1984).
[112]Yu. V. Zanevsky, S. P. Chernenko, A. V. Ivanov, *et al.*, Nucl. Instrum. Methods **153**, 445 (1978).
[113]Yu. S. Anisimov, S. P. Chernenko, A. B. Ivanov, *et al.*, J. Chromatogr. **178**, 117 (1978).

[114]Yu. S. Anisimov, Yu. V. Zanevskiĭ, A. B. Ivanov, *et al*, 18-83-668, JINR, Dubna, 1983.
[115]R. Bellazzini, A. Del Guerra, M. M. Massai, *et al.*, Nucl. Instrum. Methods **190**, 627 (1981).
[116]H. N. Ngoc, J. Jeanjean, and P. Desaunais, Nucl. Instrum. Methods **173**, 605 (1980).
[117]Yu. V. Zanevskiĭ, V. D. Peshekhonov, K. Khafner, and Tran Duc Thanh, 18-84-796, JINR, Dubna, 1984.
[118]Yu. V. Zanevskiĭ, A. B. Ivanov, V. D. Peshekhonov, and I. A. Tyapkin, R13-11310, JINR, Dubna, 1978.
[119]Yu. V. Zanevskiĭ, A. B. Ivanov, S. A. Movchan, *et al.*, Bioorganicheskaya Khimiya **10**, 776 (1984).
[120]R. Bellazzini, A. Del Guerra, M. M. Massai, and G. Spandre, Nucl. Instrum. Methods **217**, 93 (1983).
[121]S. Majewski, G. Charpak, A. Breskin, and G. Mikenberg, Nucl. Instrum. Methods **217**, 265 (1983).
[122]D. A. Abdushukurov, G. G. Abdurashidova, Tran Duc Thanh, *et al.*, Nucl. Instrum. Methods A **238**, 119 (1985).
[123]D. A. Abdushukurov, Yu. V. Zanevskiĭ, A. Merkushov, *et al.*, R18-84-758, JINR, Dubna, 1984.
[124]J. R. Helliwell, Preprint, Daresbury Laboratory, DL/SC1/P 271 E, 1981.
[125]R. Kahn, R. Fourme, B. Caudron, *et al.*, Nucl. Instrum. Methods **172**, 337 (1980).
[126]T. D. Mokul'skaya, M. A. Mokul'skiĭ, A. A. Nikitin, *et al.*, Kristallografiya **22**, 744 (1977) [Sov. Phys. Crystallogr. **22**, 427 (1977)].
[127]M. E. Andrianova, D. M. Kheiker, A. N. Popov, *et al.*, J. Appl. Crystallogr. **15**, 626 (1982).
[128]Yu. V. Zanevskiĭ, A. N. Popov, D. M. Kheĭker, *et al.*, R13-83-121, JINR, Dubna, 1983.
[129]Yu. S. Anisimov, Yu. V. Zanevskiĭ, A. B. Ivanov, *et al.*, 18-85-101, JINR, Dubna, 1985.
[130]R. Hamlin, C. Cork, A. J. Howard, *et al.*, J. Appl. Crystallogr. **14**, 85 (1981).
[131]T. D. Mokul'skaya, S. V. Kuzev, M. Yu. Lubnin, *et al.*, Kristallographiya **27**, 775 (1982) [Sov. Phys. Crystallogr. **27**, 465 (1982)].
[132]A. R. Farugi, Nucl. Instrum. Methods **217**, 19 (1983).
[133]S. E. Baru, G. I. Proviz, G. A. Savinov, *et al.*, Preprint IYaF 77-90, Novosibirsk, 1977.
[134]C. J. Borkowski and M. K. Kopp, Rev. Sci. Instrum. **39**, 1515 (1968).
[135]D. Ortendahl, V. Perez-Mendez, J. Stoker, *et al.*, Nucl. Instrum. Methods **156**, 53 (1978).
[136]J. Ballon, V. Comparat, and J. Pouxe, Nucl. Instrum. Methods **217**, 213 (1983).
[137]V. A. Vagov, A. B. Kunchenko, Yu. M. Ostanevich, and I. M. Salamatin, R14-83-898, JINR, Dubna, 1983.
[138]B. N. Anan'ev, A. M. Balagurov, V. I. Gordeliĭ, *et al.*, R13-81-857, JINR, Dubna, 1981.

Translated by Patricia Millard